Atmos. Chem. Phys. Discuss., https://doi.org/10.5194/acp-2018-895
Manuscript under review for journal Atmos. Chem. Phys.
Discussion started: 18 September 2018

Atmospheric Chemistry and Physics Discussions

Arctic marine secondary organic aerosol contributes significantly to summertime particle size distributions in the Canadian Arctic Archipelago

Betty Croft[1], Randall. V. Martin[1,2], W. Richard Leaitch[3], Julia Burkart[4,a], Rachel Y.-W. Chang[1], Douglas B. Collins[4,b], Patrick L. Hayes[5], Anna L. Hodshire[6], Lin Huang[3], John K. Kodros[6], Alexander Moravek[4], Emma L. Mungall[4], Jennifer G. Murphy[4], Sangeeta Sharma[3], Samantha Tremblay[5], Gregory R. Wentworth[4,c], Megan D. Willis[4], Jonathan P. D. Abbatt[4], and Jeffrey R. Pierce[6]

[1]Dalhousie University, Department of Physics and Atmospheric Science, Halifax, NS, B3H 4R2, Canada
[2]Harvard-Smithsonian Center for Astrophysics, Cambridge, MA, 02138, USA
[3]Environment and Climate Change Canada, Climate Research Division, Toronto, ON, M3H 5T4, Canada
[4]University of Toronto, Department of Chemistry, Toronto, ON, M5S 3H6, Canada
[5]Université de Montréal, Department of Chemistry, Montréal, QC, H3C 3J7, Canada
[6]Colorado State University, Department of Atmospheric Science, Fort Collins, CO, 80423, USA
[a]now at University of Vienna, Faculty of Physics, Aerosol Physics and Environmental Physics, Vienna, 1090, Austria
[b]now at Bucknell University, Department of Chemistry, Lewisburg, PA, 17837, USA
[c]now at Alberta Environment and Parks, Environmental Monitoring and Science Division, Edmonton, AB, T5J 5C6, Canada

Correspondence: Betty Croft (betty.croft@dal.ca)

Atmos. Chem. Phys. Discuss., https://doi.org/10.5194/acp-2018-895
Manuscript under review for journal Atmos. Chem. Phys.
Discussion started: 18 September 2018

Abstract

Summertime Arctic aerosol size distributions are strongly controlled by natural regional emissions. Within this context, we use a chemical transport model with size-resolved aerosol microphysics (GEOS-Chem-TOMAS) to interpret measurements of aerosol size distributions from the Canadian Arctic Archipelago during the summer of 2016, as part of the "NETwork on Climate and Aerosols: addressing key uncertainties in Remote Canadian Environments" (NETCARE). Our simulations suggest that condensation of secondary organic aerosol (SOA) from precursor vapors emitted in the Arctic and near Arctic marine (open ocean and coastal) regions plays a key role in particle growth events that shape the aerosol size distributions observed at Alert (82.5° N, 62.3° W), Eureka (80.1° N, 86.4° W), and along a NETCARE ship track within the Archipelago. We refer to this SOA as Arctic marine SOA (Arctic MSOA) to reflect the Arctic marine-based and likely biogenic sources for the precursors of the condensing organic vapors.

Arctic MSOA from a simulated flux (500 μg m^{-2} d^{-1}, north of 50° N) of precursor vapors (assumed yield of unity) reduces the summertime particle size distribution model-observation mean fractional error by 2- to 4-fold, relative to a simulation without this Arctic MSOA. Particle growth due to the condensable organic vapor flux contributes strongly (30-50%) to the simulated summertime-mean number of particles with diameters larger than 20 nm in the study region, and couples with ternary particle nucleation (sulfuric acid, ammonia, and water vapor) and biogenic sulfate condensation to account for more than 90% of this simulated particle number, a strong biogenic influence. The simulated fit to summertime size-distribution observations is further improved at Eureka and for the ship track by scaling up the nucleation rate by a factor of 100 to account for other particle precursors such as gas-phase iodine and/or amines and/or fragmenting primary particles that could be missing from our simulations. Additionally, the fits to observed size distributions and total aerosol number concentrations for particles larger than 4 nm improve with the assumption that the Arctic MSOA contains semi-volatile species; reducing model-observation mean fractional error by 2- to 3-fold for the Alert and ship track size distributions. Arctic MSOA accounts for more than half of the simulated total particulate organic matter mass concentrations in the summertime

Canadian Arctic Archipelago, and this Arctic MSOA has strong simulated summertime pan-Arctic-mean top-of-the-atmosphere aerosol direct (-0.04 W m^{-2}) and cloud-albedo indirect (-0.4 W m^{-2}) radiative effects. Future work should focus on further understanding summertime Arctic sources of Arctic MSOA.

1. Introduction

Aerosols have an important role in the summertime Arctic climate system. Similar to their effects in other regions, aerosols interact directly with incoming solar radiation by scattering and absorption (Charlson et al., 1992; Hegg et al., 1996; Yu et al., 2006; Shindell and Faluvegi, 2009; Yang et al., 2014) and indirectly through modification of cloud properties by acting as the seeds for cloud droplet formation (Lohmann and Feichter, 2005; McFarquhar et al., 2011). In the summertime Arctic, efficient wet removal by precipitation and the smaller extent of the polar dome limit transport of pollution from lower latitudes and maintain an atmosphere that is more pristine than in the Arctic winter and springtime (Barrie, 1995; Polissar et al., 2001; Quinn et al., 2002; Stohl, 2006; Garrett et al., 2011; Brock et al., 2011; Fisher et al., 2011; Sharma et al., 2013; Xu et al., 2017). As a result, natural regional Arctic sources make strong contributions to summertime Arctic aerosol, to the related radiative effects, and to associated uncertainties (Korhonen et al., 2008; Leck and Bigg, 2010; Heintzenberg and Leck, 2012; Karl et al., 2013; Carslaw et al., 2013; Heintzenberg et al., 2015; Croft et al., 2016a; Willis et al., 2016; Burkart et al., 2017a; Mungall et al., 2017; Willis et al., 2017; Dall'Osto et al., 2017; Breider et al., 2017; Dall´Osto et al., 2018b; Leaitch et al., 2018).

Observations indicate that aerosol particle formation and growth events occur frequently in the summertime Canadian Arctic Archipelago region (within 60-130° W and 60-85° N) (Chang et al., 2011b; Leaitch et al., 2013; Willis et al., 2016; Willis et al., 2017; Croft et al., 2016a; Burkart et al., 2017a; Burkart et al., 2017b; Collins et al., 2017; Tremblay et al., 2018). These events contribute towards shaping a summertime aerosol number size distribution that is characterized by a dominant Aitken mode (particles with diameters between 10 and 100 nm) in this region (Croft et al., 2016b), similar to observations at other pan-Arctic sites (Tunved et al., 2013; Asmi et al., 2016; Nguyen et

al., 2016; Freud et al., 2017; Gunsch et al., 2017; Heintzenberg et al., 2017; Kolesar et al., 2017). Summertime Arctic aerosol size distributions are also characterized by a suppressed accumulation mode (particles with diameters between 100 and 1000 nm) due to the efficient wet removal processes in frequently drizzling low clouds (Browse et al. 2014) and the limited transport from lower latitudes (Stohl, 2006; Law and Stohl, 2007; Korhonen et al., 2008)

Evidence points to a strong marine biogenic influence on summertime Arctic aerosols (Leck and Bigg, 2010; Chang et al., 2011a; Heintzenberg et al., 2015; Dall´Osto et al., 2018b). The oceans provide the atmosphere with many particle-relevant trace gases (Carpenter et al., 2012; Carpenter and Nightingale, 2015; Ghahremaninezhad et al., 2017; Mungall et al., 2017), as well as primary particles (Gantt and Meskhidze, 2013; Grythe et al., 2014; Wilson et al., 2015). Arctic melt ponds and melting ice are also sources of vapors such as dimethyl sulfide (DMS) (Hayashida et al., 2017; Gourdal et al., 2018), which yield condensable products following oxidation (Barnes et al., 2006) that can form and grow particles (Kirkby et al., 2011). As well, observations suggest a key role for Arctic marine secondary organic aerosol (Arctic MSOA) in the Canadian Arctic Archipelago (Willis et al., 2017; Burkart et al., 2017a; Köllner et al., 2017; Leaitch et al., 2018). The condensing vapors that contribute to particle growth by formation of secondary organics in the Canadian Arctic Archipelago may be more volatile than at lower latitudes because smaller modes (particle diameters around 20 nm) grow somewhat more slowly than larger modes (particle diameters around 90 nm) (Burkart et al., 2017a). However, these vapors are still capable of growing newly formed particles, and the details about the origin and composition of Arctic MSOA precursors are not well understood.

In this study, the terminology Arctic MSOA indicates SOA formed from any organic precursor vapors emitted in open ocean and coastal regions north of 50° N, excluding methane sulfonic acid, which we treat as a separate aerosol component, consistent with most filter-based aerosol species mass measurements. In the Canadian Arctic Archipelago, Arctic MSOA is likely strongly controlled by marine biogenic activity

(Willis et al, 2017; Leaitch et al., 2018). Due to the spatial and temporal variability, and diversity of organic precursor vapor sources and chemistry, the chemical character of Arctic MSOA is not necessarily the same as other types of MSOA arising from precursors originating in other marine regions, which could be more strongly influenced by shipping and differing types of marine biogenic activity (Facchini et al., 2008; Rinaldi et al., 2010). As well, under our definition of Arctic MSOA, the presence of Arctic MSOA is not limited to the atmospheric marine boundary layer or marine environment due to transport of precursors and Arctic MSOA to continental regions.

There are few measurements of size-resolved aerosol mass concentrations in the summertime Arctic (Zábori et al., 2015; Giamarelou et al., 2016; Tremblay et al., 2018). Such measurements can provide insight about the processes that control the size distributions. Limited observations indicate that growing Aitken-mode particles with diameters between 60 and 100 nm in the Canadian Arctic Archipelago are composed almost entirely of organics, suggesting a strong role for secondary organics (Tremblay et al., 2018). On the other hand, observations from the Svalbard region (within 74-81 °N and 10-35 °E) indicate that the smaller sub-12 nm particles are composed primarily of ammonium sulfate, suggesting that ternary nucleation and early growth involving gas-phase water, ammonia (NH_3) and sulfuric acid (H_2SO_4) play a key role in the development of nucleation-mode aerosols (particle diameters smaller than 10 nm) in the region (Giamarelou et al., 2016). In the Canadian Arctic Archipelago, summertime gas-phase NH_3 concentrations have been observed to be in the range of a few hundred pptv (Wentworth et al., 2016), levels that could contribute to initial particle formation (Napari et al., 2002; Kirkby et al., 2011; Almeida et al., 2013). Sources for NH_3 in this region are not yet fully understood, but contributors include Arctic seabird colonies, biomass burning, and possibly other terrestrial sources such as tundra ecosystems that can contribute to bi-directional exchange (Skrzypek et al., 2015; Croft et al., 2016a; Lutsch et al., 2016; Wentworth et al., 2016). In addition to NH_3, H_2SO_4 and gas-phase water, other components of nucleation mode particles (diameters less than 10 nm) could include, but are not limited to, iodine (Allan et al., 2015; Dall´Osto et al., 2018a), amines (Almeida et

al., 2013) and fragmentation of primary particles as clouds and fog evaporate (Leck and Bigg, 2010).

Given the complexity of interacting processes and source-related uncertainties described above, a coupled model-measurement-based approach enables exploration of the role of particles of biogenic origin in development of summertime aerosol size distributions in the Canadian Arctic Archipelago. In this study, we use the GEOS-Chem-TOMAS model (http://geos-chem.org) with size-resolved aerosol microphysics to interpret aerosol measurements taken during the summer of 2016 in the Canadian Arctic Archipelago, at both Alert and Eureka, in Nunavut, Canada, and also along the 2016 *CCGS Amundsen* ship track. These measurements include aerosol mass loading, total aerosol number and aerosol size distributions, some of which were taken as part of the NETwork on climate and aerosols: addressing key uncertainties in Remote Canadian Environments (NETCARE) (Abbatt et al. (in prep.)). Section 2 describes our methodology, including further details about the observations, a model description, and a summary of simulations. Section 3 interprets simulations and observations to explore the contribution of both marine primary organic aerosol (arising from sea spray) and Arctic MSOA in shaping the summertime aerosol size distributions and mass concentrations in the Canadian Arctic Archipelago. We also consider the role of ternary nucleation, the simulated contribution to particle nucleation events and size distributions, and comparison with observations. Section 3 also presents sensitivity studies to explore the role of the volatility of the Arctic MSOA during growth events, and in shaping aerosol size distributions. Finally, Sect. 3 presents estimates of the contribution of Arctic MSOA to summertime Arctic direct and indirect aerosol effects. Section 4 presents a summary, and highlights key directions for future research.

2. Methodology

2.1 Aerosol measurements in the Canadian Arctic Archipelago

Figure1 shows the locations of aerosol measurements, taken at both Alert (82.5° N, 62.3° W) and Eureka (80.1° N, 86.4° W), in Nunavut, Canada and along the 2016 ship track of the *CCGS Amundsen* through the Canadian Arctic Archipelago that we interpret using the GEOS-Chem-TOMAS model. The measurements at Alert, Nunavut, Canada are made at the Global Atmospheric Watch (GAW) observatory. Weekly samples of ambient aerosol are collected on Teflon filters, using a cyclone to limit particles to diameters smaller than 1 μm (PM1.0), and analyzed by ion chromatography for several inorganic ions including sulfate, ammonium, nitrate, and methane sulfonic acid (MSA). Further details are provided in Leaitch et al. (2013) and Li and Barrie (1993). Weekly samples are also collected on quartz filters behind the cyclone (PM1.0) and analyzed for organic and elemental carbon by thermal volatilization and combustion (Huang et al., 2006), as described in Sharma et al. (2017) and Leaitch et al. (2018). There is a possibility that volatile organic carbon (VOC) vapors could also be absorbed on the quartz filters (Leaitch et al., 2018). As a result, we view these measurements as an upper limit on organic carbon mass concentrations at Alert as discussed further in Sect. 3.1. Since 2011, hourly-mean size distributions for particles with diameters from 20 to 500 nm are measured at Alert using a TSI 3034 Scanning Mobility Particle System (SMPS), which is verified for sizing on site using mono-disperse particles of polystyrene latex and of ammonium sulfate generated with a Brechtel Manufacturing Incorporated Scanning Electrical Mobility Spectrometer. Total particle number concentration for particles larger than 10 nm in diameter is measured at Alert with a TSI 3772 Condensation Particle Counter (CPC). The CPC and SMPS agree to within 10% when all particles are large enough to be counted by both instruments. Data that could be influenced by local camp activities are filtered from the data set by removing data 1) when the wind direction was within a 45° angle centred on the Alert camp; 2) during line zeroes to check the connections to the instruments and any other repetitive occurrence that might influence the measurements; 3) when logs indicated potential sources nearby (e.g. trucks); and 4) to account for unknown factors, when data spikes remain that lasted two hours or less.

At Eureka, Nunavut, Canada, aerosol measurements are taken at the RidgeLab of the Polar Environment Atmospheric Research Laboratory (PEARL) (Fogal et al., 2013),

Atmos. Chem. Phys. Discuss., https://doi.org/10.5194/acp-2018-895
Manuscript under review for journal Atmos. Chem. Phys.
Discussion started: 18 September 2018

which is located on Ellesmere Island at 610 m above sea level and about 480 km southwest of Alert. Since 2015, size distributions for particles with diameters between 10 and 500 nm have been measured at the RidgeLab using a TSI 3034 SMPS. Data are recorded every three minutes and averaged to hourly means. Further details about the instrument and sampling are presented in Tremblay et al. (2018).

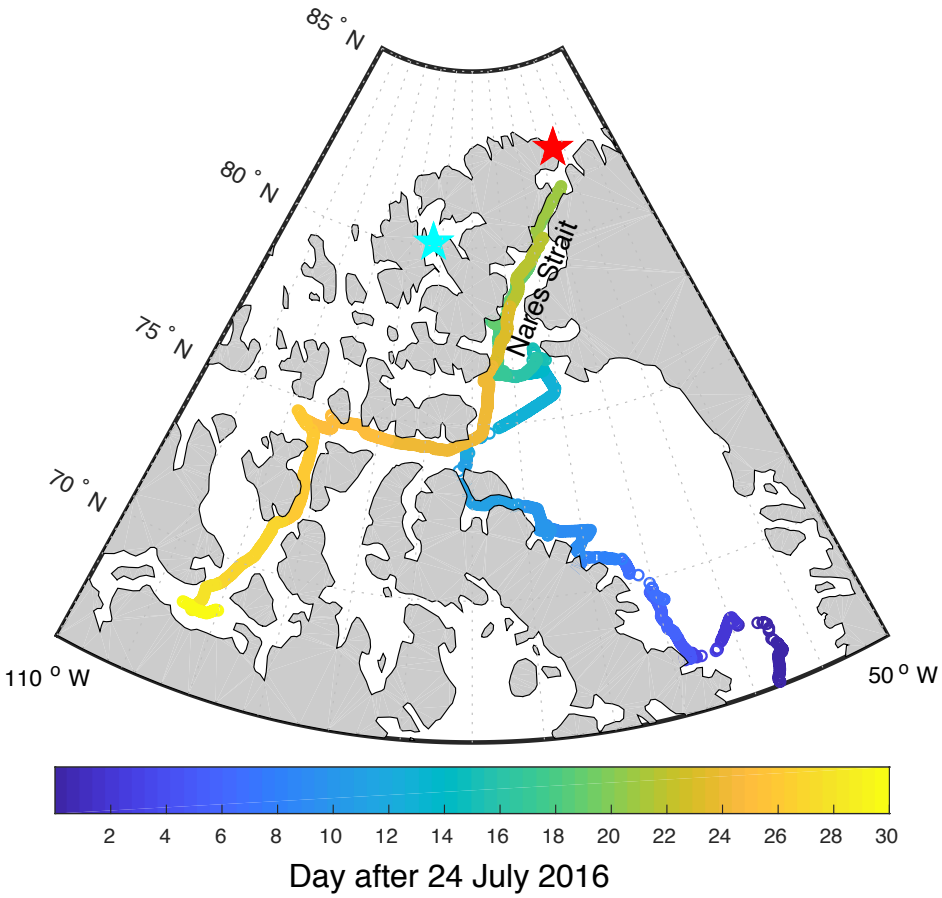

Figure 1: *CCGS Amundsen* 2016 cruise track through Canadian Arctic Archipelago color coded by the number of days after 24 July 2016. Land is shaded in grey. Location of Alert and Eureka shown by red and cyan stars, respectively.

During the summer of 2016, the research icebreaker *CCGS Amundsen* travelled through the Canadian Arctic Archipelago as a part of the NETCARE project (Abbatt et al. (in

prep)). Figure 1 shows the cruise track for 24 July - 23 August 2016. During the cruise, total number concentrations of aerosols with diameters larger than 4 nm were measured with a TSI 3776 ultrafine condensation particle counter (UCPC). Aerosol size distributions for particles with diameters between 10 nm to 430 nm were measured with a TSI 3080/3087 SMPS. Data collected while the wind direction was less than 60° to port and less than 90° to starboard of the ship's orientation were accepted for further analysis. We consider all measurements taken over 23 July 2016 to 24 August 2016, when the ship was north of 66° N. Further details about the instrumental setup and sampling are in Collins et al. (2017). Measurements of NH_3 were also taken during the cruise with a Quantum Cascade Tunable Infrared Laser Differential Absorption Spectroscopy (QC-TILDAS) analyzer (Ellis et al., 2010). The instrument has a fast response time that enabled measurements at 1 Hz during the cruise, with measurements taken from 29 July 2016 to 23 August 2016. NH_3 data were also filtered for wind direction, ship speed and measured aerosol number concentrations to exclude periods that indicated influence from the ship exhaust.

Tundra samples were collected in triplicate from three sites near Alert, NU on 14 and 15 July 2016 to estimate tundra NH_3 emission potential. The sites ranged from approximately 1 to 9 km west of the GAW observatory. Sampling and subsequent analysis for ammonium concentration ($[NH_4^+]$) and pH were carried out according to Wentworth et al. (2014). From mid June to the end of July 2016, hourly measurements of tundra temperature were recorded adjacent to the GAW observatory using commercially available soil temperatures sensors (iButtons, Maxim Integrated). Tundra $[NH_4^+]$, pH, (both based on the 14 and 15 July 2016 soil samples) and hourly temperature were used to calculate the hourly NH_3 tundra compensation, which reflects the predicted equilibrium NH_3 concentration in the atmosphere above the tundra (Wentworth et al., 2014). A tundra-air exchange velocity was calculated using a resistance-in-series scheme with parameterizations from Wesley (1989) and Walker et al. (2014). The average NH_3 emissions at the three sites were then calculated as the mean of the products of the exchange velocity and compensation point, resulting in estimated emission rates of 0.12, 1.4, and 2.2 ng m^{-2} s^{-1}. Here, we adopt the highest value to provide an upper estimate on

the contribution of the tundra to atmospheric NH_3. It should be noted that extrapolating calculated emissions from discrete tundra samples to the entire Canadian Arctic Archipelago carries a very large degree of uncertainty. However, the paucity of necessary tundra measurements and the lack of any terrestrial Arctic NH_3 fluxes prevent a more rigorous approach.

2.2 Model description

The GEOS-Chem (GC) chemical transport model version v10-01 (http://geos-chem.org) coupled to the TwO-Moment Aerosol Sectional (TOMAS) microphysics model (Adams and Seinfeld, 2002; Kodros et al., 2016; Kodros and Pierce, 2017) is employed in this study. Our model version has 47 vertical levels and a 4° x 5° horizontal resolution. The GEOS-FP reanalysis (http://gmao.gsfc.nasa.gov) provides the meteorological fields. We use a TOMAS version with 15 size sections, including dry diameters ranging from 3 nm to 10 µm (Lee and Adams, 2012). Tracers within each size bin include particle number and mass of sulfate, black carbon (hydrophobic and hydrophilic), organic carbon (hydrophobic and hydrophilic), sea salt, dust and water. All simulations are for the months of July and August 2016, with a one-month spin-up during June that is not included in our analysis.

2.2.1 TOMAS aerosol microphysics

The TOMAS aerosol microphysics scheme employed in our simulations has 13 logarithmically spaced size sections for aerosol dry diameters from approximately 3 nm to 1 µm, and 2 additional size sections to represent aerosol dry diameters from 1 to 10 µm (Lee and Adams, 2012). Particle formation is treated according to the ternary H_2SO_4–NH_3–H_2O nucleation scheme described by Baranizadeh et al. (2016). The formation rate of particles at about 1.2 nm in mass diameter is determined from a full kinetics simulation by Atmospheric Cluster Dynamics Code (ACDC) (Olenius et al., 2013) using particle evaporation rates based on quantum chemistry. The scheme is implemented as a look-up

table as a function of gas-phase H_2SO_4 and NH_3 concentrations, relative humidity, temperature and condensation sink for condensable vapors. Growth and loss of particles smaller than 3 nm are approximated with the Kerminen et al. (2004) scheme. Implementation of this scheme is supported by the findings of Giamarelou et al. (2016) that nucleation-mode particles in the summertime Arctic are predominantly ammoniated sulfates. All simulations use the Brownian coagulation scheme of Fuchs (1964) and consider coagulation between all particle sizes, an important sink for particle number, particularly for those particles with diameters smaller than 100 nm. Coagulation between aerosols contained in cloud hydrometeors and interstitial aerosols is parameterized as described in Pierce et al. (2015). An overview of the condensational-growth assumptions follows the discussion of inventories and secondary organic aerosol (SOA) scheme below.

2.2.2 Natural emissions

Several natural emissions inventories and parameterizations are used in our study. Emissions of dimethyl sulfide (DMS) are based on the seawater DMS climatology of Lana et al. (2011) with modifications for the Canadian Arctic Archipelago region as described in Mungall et al. (2016), who found that the climatology seawater DMS was biased low relative to observations from summer 2014. The air-water transfer velocities for DMS are based on the scheme of Johnson (2010). Natural sources of NH_3, along with biofuel and anthropogenic sources are from the Global Emissions InitiAtive (GEIA) (Bouwman et al., 1997). For some of our simulations, as described in Sect. 2.3, Arctic seabird colony NH_3 emissions are implemented following Riddick et al. (2012a), Riddick et al (2012b), Croft et al. (2016a) and Wentworth et al. (2016). Our simulations also implement an NH_3 source from Arctic tundra with a fixed emission rate of 2.2 ng m^{-2} s^{-1}, an upper estimate based on inferred bi-directional exchange fluxes calculated using soil measurements made during the summer of 2016 near Alert, which found the tundra can act as a source of NH_3 to the atmosphere (Murphy et al. (in prep)). Given the uncertainty in the tundra source, this source can be viewed as a surrogate for the missing emissions needed to bring the simulated NH_3 mixing ratios to agreement with measurements as

discussed in Sect. 3.1. Additionally, natural sources of NH_3 and organic carbon (OC) aerosol are included in the biomass burning emissions from the 3-hourly Global Fire Emissions Database, version 4 (GFED4) for 2016 (Giglio et al., 2013; Van Der Werf et al., 2017), which is employed in all simulations. Dust emissions employ the Dust Entrainment and Deposition (DEAD) scheme of Zender et al. (2003), developed in GEOS-Chem by Fairlie et al. (2007).

Emissions of sea spray in our simulations are based on the Mårtensson et al. (2003) parameterization. We view this parameterization as yielding an upper bound on ultrafine primary marine emissions. Comparisons with the Jaeglé et al. (2011) parameterization, employed in the standard GEOS-Chem-TOMAS model, indicate that the Mårtensson et al. (2003) parameterization yields greater sub-100 nm fluxes by up to a few orders of magnitude (Jaeglé et al., 2011). This choice of emissions inventory enables evaluation of the contribution of sea-spray to simulated ultrafine particle concentration under one of the inventories that is most favorable to ultrafine sea-spray particle production. Additionally, as opposed to assuming that all sea spray is sodium chloride, we emit sea spray particles with diameters smaller than 100 nm as hydrophobic organic carbon aerosol and particles larger than 100 nm as sodium chloride. This modification was introduced based on measurements indicating that sub-100 nm sea spray particles are composed mostly of organics, whereas larger particles have a progressively more dominant salt component (Collins et al., 2013; Prather et al., 2013; Gantt and Meskhidze, 2013; Quinn et al., 2015). However, knowledge gaps remain related to the spatial distribution of sea spray composition and hygroscopicity (Collins et al., 2016).

2.2.3 Anthropogenic emissions

Our simulations also include global anthropogenic emissions from the Emissions Database for Global Atmospheric Research (http://edgar.jrc.ec.europa.eu/archived_datasets.php) (EDGAR) inventory. The EDGAR inventory is overwritten by regional inventories for Europe (European Monitoring and Evaluation Program (EMEP) (Crippa et al., 2016)), Canada (Criteria Air Contaminant

Inventory), the United States (National Emission Inventory (NEI)), and Asia (MIX inventory (Li et al., 2017)). As well, the Bond et al. (2007) inventory overwrites the EDGAR fossil-fuel and biofuel emissions for black and organic carbon.

2.2.4 Chemical mechanism

The GEOS-Chem-TOMAS chemical mechanism represents the reactions of more than 100 gas-phase species, including particle-relevant reactions such as DMS oxidation by the hydroxyl radical (OH) to produce sulfur dioxide (SO_2) by both the addition and abstraction channels, and also reaction with the nitrate radical (NO_3) (Chatfield and Crutzen, 1990; Chin et al., 1996; Alexander et al., 2012). SO_2 then undergoes either gas-phase reactions with OH to produce H_2SO_4 or aqueous oxidation with either hydrogen peroxide (H_2O_2) or ozone (O_3) to produce particulate sulfate. For the aerosol microphysics scheme, gas-phase H_2SO_4 can join with water vapor and gas-phase NH_3 for ternary nucleation of nascent particles, and it can also condense to grow pre-existing particles. The sulfate produced by aqueous-phase reactions is added to particles that are large enough to have activated to form cloud droplets, only contributing to the growth of these larger particles. In general, particles with diameters of 50 nm or larger activate in our simulations, although observations from the Canadian Arctic Archipelago indicate that particles as small as 20 nm could activate under some conditions (Leaitch et al., 2016). Methane sulfonic acid (MSA) that is produced by the DMS-OH-addition channel contributes to condensational growth of existing particles, as described in Hodshire et al. (in prep), but does not contribute to particle nucleation in our simulations. In this study, we did not include additional chemistry related to production of dimethylsulfoxide (DMSO). As a result, our simulated yields of MSA may be slightly underpredicted, and sulfate formation slightly overpredicted (Breider et al., 2014).

2.2.5 Secondary organic aerosol scheme

Arctic MSOA is treated with the simplified SOA scheme developed by Kim et al. (2015), which for all simulations includes SOA precursors from non-marine sources associated

with terrestrial biogenic, fossil fuel, biofuel, and biomass burning emissions. The scheme introduces two additional tracers, a gas-phase SOA precursor, and a SOA tracer that is available to condense on the particles. The gas-phase SOA precursor oxidizes to form SOA on a fixed timescale of 1-day. For biogenic sources the emissions are distributed between these two tracers with a 50/50 split to represent the fast oxidation timescale of biogenic precursors of typically shorter than 1 day. The model employed for this study does not include aqueous-phase production of SOA. As a part of our sensitivity simulations (described in Sect. 2.3), additional fixed-flux organic vapor emissions yielding Arctic MSOA are implemented in the region north of 50° N over open seawater with a 50/50 split between the gas-phase precursor and the phase that is available for condensation.

While our simulations do not include initial formation of nascent particles by clusters of organic vapors, we do allow growth of particles by condensation of organic vapors, as well as by condensation gas-phase H_2SO_4 and MSA. In the standard model, all vapors condense proportional to the Fuchs-corrected aerosol surface area distribution, behaving like a non-volatile condensing gas (Donahue et al., 2011; Pierce et al., 2011; Riipinen et al., 2011; Liu et al., 2016; Tröstl et al., 2016; Ye et al., 2016). The important role of organic condensation was found at lower latitude continental sites (Riipinen et al., 2011). Our simulations investigate this role for the Arctic. We also conduct additional sensitivity simulations (described in Sect. 2.3), which allow condensation of a fraction of the vapors according to the mass distribution, behaviour like a semi-volatile as opposed to non-volatile condensing organic.

2.2.6 Wet and dry deposition

Removal of simulated aerosol mass and number occurs by both wet and dry deposition. The wet deposition parameterization includes both in-cloud and below-cloud scavenging as developed by Liu et al. (2001) and Wang et al. (2011), with modifications as described in detail in Croft et al. (2016b) to more closely link the wet removal to the meteorological fields for cloud liquid, ice water content, and cloud fraction. To represent the impact of

drizzle from summertime Arctic low-level clouds, we implemented wet removal from all Arctic clouds below 500 m using a fixed efficiency of 0.01 s^{-1}, similar to the approach of Browse et al. (2012). In-cloud wet removal in GEOS-Chem-TOMAS is limited to the size range that can activate to form cloud hydrometeors. Size-dependent dry deposition uses the resistance in series approach of Wesley (1989). Simulated gas-phase species are also removed by dry and wet deposition as described in Amos et al. (2012). Removal depends on solubility such that aerosol precursors including ammonia, and sulphur dioxide are removed by precipitation, while SOA precursors and dimethyl sulphide are not.

2.2.7 Radiative calculations

The following radiative transfer calculations are conducted off-line using the simulated summertime-mean aerosol mass and number concentrations to examine the effects of organic condensation. For calculation of the direct radiative effect (DRE), aerosol optical depth, single-scattering albedo and asymmetry factor are calculated with Mie code (Bohren and Huffman, 1983) and use refractive indices from the Global Aerosol Dataset (GADS) (Koepke et al., 1997). These optical properties, along with cloud fraction and surface albedo from GEOS-FP assimilated meteorology are input to the Rapid Radiative Transfer Model for Global Climate Models (RRTMG) (Iacono et al., 2008), to determine the change in top-of-the-atmosphere solar flux between two simulations, treating all particles except black carbon as internally mixed and spherical.

We also calculate the cloud-albedo aerosol indirect effect (AIE) with the method described in Croft et al. (2016a) and Kodros et al. (2016). The cloud droplet number concentration (CDNC) is calculated off-line using the parameterization of Abdul-Razzak and Ghan (2002), again using the summertime mean aerosol mass and number concentrations from our simulations. We assume an updraft velocity of 0.5 m s^{-1} and treat all aerosols as internally mixed to determine the hygroscopicity parameter of Petters and Kreidenweis (2007). For each model grid box, we assume cloud droplet radii (r) of 10 μm and perturb this value with the ratio of summertime-mean CDNC from simulations

(acronyms described in Table 1 and simulations described in Sect. 2.3), following Rap et al. (2013), Scott et al. (2014) and Kodros et al. (2016),

$$r_{perturbed} = 10\left(\frac{CDNC_{BASE+TUNDRA+BIRDS+100xnuc}}{CDNC_{BASE+TUNDRA+BIRDS+100xnuc+AMSOAnv/sv}}\right)^{1/3}. \quad (1)$$

Then RRTMG is used to determine the change in top-of-the-atmosphere solar flux attributed to the change in effective cloud droplet radii, again using the summertime meteorological data from GEOS-FP. Our AIE calculation is limited to this single aerosol indirect effect; the impact of Arctic MSOA on additional indirect effects (Lohmann and Feichter, 2005) requires further investigation in future studies.

2.3 Overview of simulations

Our simulations are conducted with a focus on interpreting the summertime 2016 aerosol measurements from the Canadian Arctic Archipelago. These simulations are used to explore the role of biogenic sources in shaping the aerosol size distributions by the processes of nucleation of particles from gas-phase molecules followed by growth, with a focus on Arctic MSOA. We also consider the role of marine primary particle emissions.

Table 1 presents simulation acronyms used in the following discussion. Simulation BASE employs the standard GEOS-Chem-TOMAS model described in Sect. 2.2. We examine the potential contribution of regional terrestrial NH_3 sources to aerosol size distributions with simulations BASE+BIRDS, BASE+TUNDRA, and BASE+TUNDRA+BIRDS. Simulation BASE+BIRDS implements seabird-colony NH_3 emissions of 35 Gg spread uniformly in time between 1 May and 30 September, based on the Riddick et al. (2012a) and Riddick et al. (2012b) inventory with modifications and spatial distribution as described in Croft et al. (2016a) and Wentworth et al. (2016). Simulation BASE+TUNDRA includes a fixed NH_3 emission of 2.2 ng m^{-2} s^{-1} from all Arctic tundra as discussed in Sect. 2.2.2. Simulation BASE+TUNDRA+BIRDS uses both the seabird colony and tundra NH_3 sources.

Simulation Acronyms	Description
BASE	Base simulation, described in detail in Sect. 2.2.
BIRDS	Seabird-colony ammonia emissions included
TUNDRA	Tundra ammonia emissions included
AMSOAnv	Non-volatile Arctic MSOA
AMSOAnv/sv	30% non- and 70% semi-volatile Arctic MSOA
2xAMSOAnv/sv	Double organic vapor emissions of AMSOAnv/sv
100xnuc	Particle formation rate scaled by 100-fold

Table 1: Description of acronyms that are used in the simulation names. Simulations are described in detail by full simulation name in Sect. 2.3.

Simulation BASE+TUNDRA+BIRDS+AMSOAnv adds a source of Arctic MSOA. This source draws upon measurements presented by Mungall et al. (2017) indicating that the marine microlayer is a source of oxygenated volatile organic compounds (OVOCs), key precursors to secondary organic aerosol. Furthermore, Willis et al. (2017) identified a positive relationship between the ratio of organic to sulfate aerosol mass concentrations and time spent over open water, suggesting a marine SOA source. Studies from other regions also identified biogenic VOCs of marine origin, but their marine sources are not fully identified (Carpenter and Nightingale, 2015; Tokarek et al., 2017; Chiu et al., 2017). Likewise for the Arctic, the emission rates for these vapors are not well understood (Burkart et al., 2017a). Given this uncertainty, we identified a fixed Arctic MSOA-precursor vapor source flux (Arctic MSOA formed with a mass yield of unity) from the ice-free seawater in the Arctic and near Arctic (north of 50° N). The marine organic vapors are emitted into the simplified SOA scheme described in Sect. 2.2.5 with a 50/50 split between precursor gas (with a 1-day lifetime before forming SOA) and vapor that instantly condenses to particles in the marine boundary layer. This split represents variability in the VOCs lifetime for aging to sufficiently low volatility that they can condense on the particulate phase. At the point of condensation, we assume the vapors to be effectively non-volatile, with condensation according to the Fuchs-corrected surface area. A top-down estimate of the flux (500 μg m^{-2} d^{-1}; simulated flux magnitude of 468 μg

m^{-2} d^{-1} north of 50° N, reported to one significant figure due to uncertainty) is adopted that best represents observations as shown in the following sections within the context of our simulations, which are an upper limit on primary organic aerosol contribution. To put the implemented flux in context, this is within an order of magnitude of the isoprene flux estimated from a north temperate deep lake (Steinke et al., 2018). Future work should include a bottom-up estimate of the SOA-precursor source flux.

Simulation BASE+TUNDRA+BIRDS+100xnuc+AMSOAnv examines the impact of particle precursors in addition to H_2SO_4, NH_3 and water that could nucleate nascent particle clusters in the Arctic. These precursors could include (but are not limited to) gas-phase iodine (Allan et al., 2015; Dall´Osto et al., 2018a), amines (Almeida et al., 2013) and organics (Riccobono et al., 2014). It is unclear if marine biological activity creates organic vapors that participate in particle nucleation. Disintegration of larger particles from evaporating clouds and fog could contribute to the number of nascent particles (Leck and Bigg, 2010). Unfortunately, a nucleation parameterization does not exist that is suitable to include interactions of all these materials simultaneously (Riccobono et al., 2014; Dunne et al., 2016; Gordon et al., 2017). To explore these effects, we scale up the ternary nucleation by 100-fold to represent the potential effects of particle precursors with similar spatial origin to those involved in ternary nucleation. Almeida et al. (2013) and Riccobono et al. (2014) observed increases in nucleation rates by about 100-fold above the sulfate-ammonia-water vapor system when amines or monoterpene-oxidation products were added. We treat the 100-fold increase as an estimate of how additional materials could enhance nucleation. We also conduct simulation BASE+TUNDRA+BIRDS+100xnuc, which is otherwise similar to BASE+TUNDRA+BIRDS+100xnuc+AMSOAnv, but without the condensable marine organic vapors.

Finally, we conduct simulations to examine the impact of Arctic MSOA volatility. Burkart et al. (2017a) found that condensing gas-phase materials in the Canadian Arctic Archipelago were surprisingly more volatile than at lower latitudes. Simulation BASE+TUNDRA+BIRDS+100xnuc+AMSOAnv/sv is similar to simulation

BASE+TUNDRA+BIRDS+100xnuc+AMSOAnv, except that 30% of the Arctic MSOA behaves as non-volatile compounds and condenses according to Fuchs-corrected surface area, whereas 70% of the Arctic MSOA behaves as idealized semi-volatile compounds and condenses according to the particle mass distribution (quasi-equilibrium condensation). This is a larger fraction of semi-volatile vapors than the 50/50 semi-/non-volatile split employed by Riipinen et al. (2011) for lower latitude continental sites, and consistent with the findings of Burkart et al. (2017a) for the Canadian Archipelago region that the condensing vapors were more semi-volatile than at lower latitudes. Simulation BASE+TUNDRA+BIRDS+100xnuc+2xAMSOAnv/sv is similar to simulation BASE+TUNDRA+BIRDS+100xnuc+AMSOAnv/sv, except that for the former, we double the flux of marine organic vapors to examine the impact of a change in flux since the geographic distribution of the source rate is highly uncertain.

We calculate the mean fraction error (MFE) (Boylan and Russell, 2006) between our simulations and observed aerosol size distributions using the following equation.

$$\mathrm{MFE} = \frac{1}{N}\sum_{i=0}^{i=N} \frac{abs|C_m(i)-C_o(i)|}{(C_m(i)+C_o(i))/2} \qquad (2)$$

where $C_m(i)$ is the integrated value for the ith moment of the simulated aerosol size distribution and $C_o(i)$ is the integrated value for the ith moment of the observed size distribution, for the N moments (zeroth to third). Fractional bias is calculated likewise, but without the absolute value of the numerator.

3. Results and Discussion

3.1 Summertime aerosol mass concentrations at Alert

Table 2 shows the observed climatological- (data available for years 2011 to 2015), summertime- (July and August) mean mass concentrations for organic carbon (OC), NH_4^+, sulfate ($SO_4^=$) and MSA from filter measurements at Alert and also the summertime mean for our 9 simulations (all for 2016). These long-term observations at

Alert provide a useful climatology for comparison with our simulations, even if not for the same years. An organic matter (OM) to OC ratio of 2.1 was applied to convert the simulated OM to OC. There is uncertainty in the OM/OC ratio, which can range from about 1.4 to 2.4; however, the larger values are generally associated with rural and remote regions (Turpin and Lim, 2001; Russell, 2003; Philip et al., 2014). This ratio (2.1) is within 4% of summertime-mean OM/OC ratios from the Organic Functional Groups (OFG) measurements from available years (2012-2014) at Alert that are detailed in Leaitch et al. (2018). Simulation BASE underpredicts the observed annual mean OC mass concentrations by a factor of about 3, and is below the inter-annual range shown in Table 2. The simulated OC is strongly sensitive to Arctic MSOA, increasing by a factor of 2.5 for simulation BASE+TUNDRA+BIRDS+AMSOAnv relative to simulation BASE+TUNDRA+BIRDS, to yield better consistency with the measurement mean. As described in Leaitch et al. (2018), these measurements could also include organics from condensation of volatile organic compounds directly onto the quartz filters, contributing to a factor of 1.1-2.5 increase in concentrations relative to OFG analysis by Fourier transform infrared (FTIR) spectroscopy. This is only one of the potential issues with determining OC based on sampling at such low concentrations over one week. Furthermore, the measurement OC mass concentrations were not available for the year of our simulations, and inter-annual variability in summertime OC is large. As a result of these complexities, we also compare between the year-matched simulated and SMPS volume distributions (Sect. 3.3), which we consider to be a more robust evaluation of the simulated particle mass concentrations.

The simulated OC mass concentration is also sensitive to the rate of formation of nascent particles in our simulations. With an increase in nucleation rate, as in simulation, BASE+TUNDRA+BIRDS+100xnuc+AMSOAnv relative to simulation BASE+TUNDRA+BIRDS+AMSOAnv, the simulated OC mass concentrations increase by about 15% because there are more nucleation- and Aitken-mode particles available to 'catch' the condensing vapors, and these smaller particles are less efficiently removed by wet scavenging. Additionally, the simulations of OC mass concentrations are sensitive to the assumed volatility of the Arctic MSOA. For the 30/70 split of non-volatile and semi-

volatile vapors as in simulation BASE+TUNDRA+BIRDS+100xnuc+AMSOAnv/sv, the OC mass concentrations are reduced by about 15% relative to simulation BASE+TUNDRA+BIRDS+100xnuc+AMSOAnv. The semi-volatile vapors condense to larger particles (Pierce et al., 2011; D'Andrea et al., 2013; Hodshire et al. (in prep.)) that are more efficiently removed by precipitation. The emissions flux of Arctic MSOA-precursor vapors has a nonlinear impact on the simulated OC mass concentrations. Table 2 shows that the change in mean OC concentrations differs between simulation pairs with the same absolute change in Arctic MSOA-precursor emissions (simulations BASE+TUNDRA+BIRDS+100xnuc+2xAMSOAnv and BASE+TUNDRA+BIRDS+100xnuc+AMSOAnv, relative to BASE+TUNDRA+BIRDS+100xnuc+AMSOAnv and BASE+TUNDRA+BIRDS+100xnuc).

	OC	**NH_4^+**	**MSA + $SO_4^=$**
Observations	85.0 (37.7, 132.9)	16.3 (7.6, 31.2)	58.8 (30.8, 97.5)
Simulations			
BASE	28.7	2.8	54.8
Extra Ammonia			
BASE+BIRDS	27.9	12.6	56.6
BASE+TUNDRA	27.0	20.0	58.5
BASE+TUNDRA+BIRDS	33.3	22.6	66.2
Arctic MSOA (non-volatile)			
BASE+TUNDRA+BIRDS+AMSOAnv	72.0	22.0	64.8
Extra Nucleation			
BASE+TUNDRA+BIRDS+100xnuc	33.2	23.5	69.2
BASE+TUNDRA+BIRDS+100xnuc+AMSOAnv	82.0	24.1	72.1
Arctic MSOA Volatility (mix non-/semi-volatile)			
BASE+TUNDRA+BIRDS+100xnuc+AMSOAnv/sv	70.2	23.6	69.7
BASE+TUNDRA+BIRDS+100xnuc+2xAMSOAnv/sv	104.6	23.4	68.7

Table 2: July and August mean aerosol mass concentrations (ng m^{-3}) at Alert from measurements (2011-2015) (brackets show the minimum and maximum annual mean over the measurement period) and GEOS-Chem-TOMAS simulations (2016) as described in Table 1 and Sect. 2.3 for organic carbon (OC), ammonium (NH_4^+), and methane sulfonic acid (MSA) and sulfate ($SO_4^=$).

We also evaluated the simulation of relevant inorganic ions. Simulation BASE strongly underpredicts measured ammonium concentrations by a factor of 8. Implementation of

the seabird-colony and tundra NH_3 sources (simulation BASE+TUNDRA+BIRDS) yields closer model-measurement agreement (within about 40%), although this is a challenging simulation given the uncertainties in the NH_3 sources within these remote regions. Relative to measurements taken during the summer 2016 cruise track, simulation BASE also underpredicts grid-box mean NH_3 mixing ratios with a mean fractional bias (MFB, described in Sect. 2.3) (Boylan and Russell, 2006) of -1.98, which is reduced for simulations BASE+BIRDS (-1.23), BASE+TUNDRA (-0.22), and BASE+TUNDRA+BIRDS (+0.06).

Implementation of seabird-colony and tundra NH_3 sources (simulation BASE+TUNDRA+BIRDS) also increases the simulated summertime (July and August) mean sulfate concentrations by about 20% over simulation BASE. The extra free NH_3 (simulation BASE+TUNDRA+BIRDS relative to BASE) promotes particle nucleation, which decreases the mean diameter of the particles available for H_2SO_4 condensation as sulfate, slowing sulfate wet scavenging as the smaller particles have less efficient removal. Scaling up the nucleation rate further increases the sulfate concentrations by about 10-15% as the concentrations of nucleation- and Aitken-mode particles are further increased, further reducing the mean diameter of the particles available for condensation of H_2SO_4, and slowing wet scavenging of sulfate. All simulations are within 20% of the measured sulfate concentrations. As well, we evaluated the model-measurement agreement for sodium ions and found agreement within a factor of two for all simulations. These mass-based comparisons offer confidence that the simulations which include Arctic MSOA are reasonable. In the following sections, we consider the impact of Arctic MSOA on total aerosol number concentrations and the moments of the aerosol size distributions.

3.2 Total aerosol number concentrations along the 2016 ship track and at Alert

Figure 2 shows time series measurements during August 2016 of total particle number concentration for particles with diameters larger than 4 nm conducted from the *CCGS Amundsen* (Collins et al., 2017) and for particles with diameters larger than 10 nm at

Atmos. Chem. Phys. Discuss., https://doi.org/10.5194/acp-2018-895
Manuscript under review for journal Atmos. Chem. Phys.
Discussion started: 18 September 2018

Alert. The measurement time series shows episodic bursts of particle number concentration greater than 500 cm^{-3}. Interestingly, at several times the elevated number concentrations occur at both Alert and at the ship, such as on August 3, 8, 9, 10, 11, 15 and 16. Both time series also show relatively lower total number concentrations on August 5 and August 13 to 14, when there was precipitation, and when the ship was in the Nares Strait region shown on Fig.1.

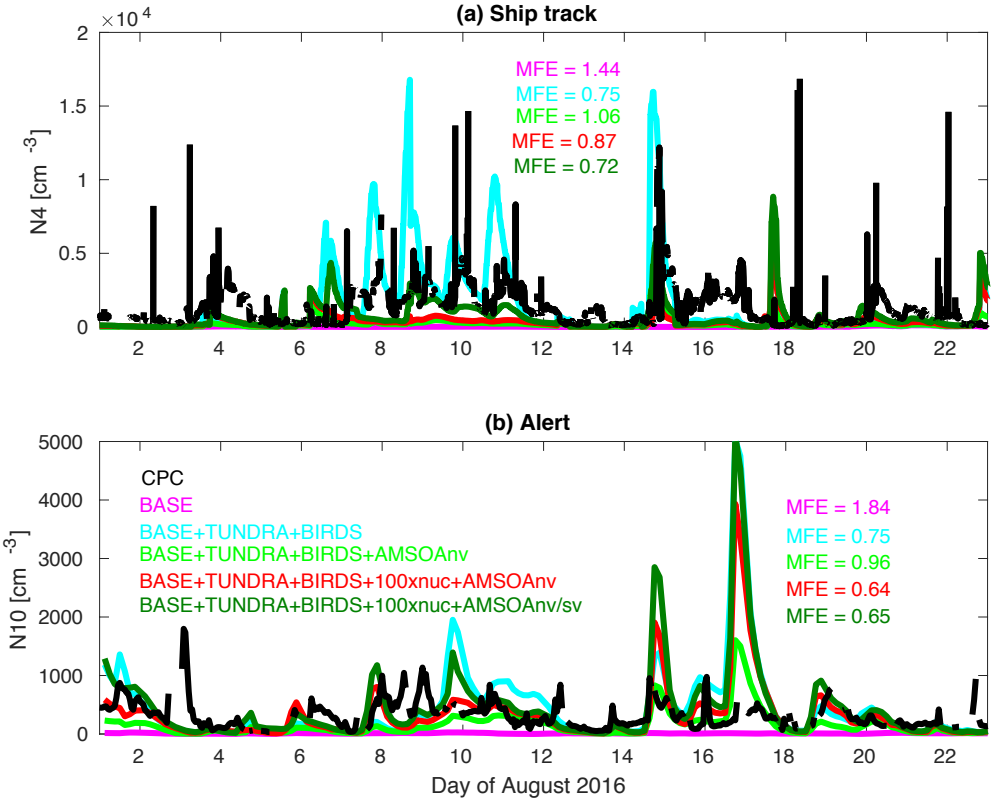

Figure 2: Time series for August 2016 observed number concentration from condensation particle counter (CPC) for aerosols with (a) diameters larger than 4 nm (N4) along Amundsen ship track (Fig. 1) and (b) diameters larger than 10 nm (N10) at Alert (described in Sect. 2.1) and for the simulations as described in Table 1 and Sect. 2.3 (color coded as shown on legend). MFE: mean fractional error between observations and simulations, color-coded to match simulation names.

Figure 2 also shows the time series of coincidently sampled simulated number concentrations for five of the simulations described in Table 1 and Sect. 2.3. We calculated the model-to-measurement mean fractional error (MFE) (Eq. (2)) for the

simulations of total number concentration shown on Fig. 2. The BASE simulation is associated with the greatest MFE values for the ship track (1.44) and Alert (1.84). The simulations better capture the bursts of particle number when including NH_3 sources from seabird colonies and tundra, similar to the findings of Croft et al. (2016a) with MFE values reduced to 0.75 for both the Alert and ship track time series for simulation BASE+TUNDRA+BIRDS.

Implementation of Arctic MSOA in simulation BASE+TUNDRA+BIRDS+AMSOAnv increases the MFE relative to simulation BASE+TUNDRA+BIRDS, to 1.06 for the ship track and 0.96 for the Alert time series. This MFE increase occurs because more vapors are available to condense on to the particle surface area, building the condensation sink for H_2SO_4, which reduces the simulated formation of nascent particles by ternary nucleation with H_2SO_4. These effects reduce the number of ultrafine particles, similar to that described by D'Andrea et al. (2013), who investigated the impact of anthropogenically enhanced SOA for a set of sites distributed around the world.

Scaling the nucleation rate by 100-fold reduces the MFE to 0.87 for the ship track and 0.64 at Alert, for simulation BASE+TUNDRA+BIRDS+100xnuc+AMSOAnv. This scaling acts as a surrogate for the parameterization of particle nucleation by materials in addition to the simulated gas-phase NH_3, H_2SO_4 and water, as described in Sect. 2.3. This increased nucleation rate enables ultrafine particles to become more numerous, despite the increased condensation sink associated with the implemented Arctic MSOA source.

Considering both the 2016 ship track and Alert time series together, the lowest MFE pair is found for simulation BASE+TUNDRA+BIRDS+100xnuc+AMSOAnv/sv, 0.72 and 0.65, respectively. This simulation treats the Arctic MSOA as a 30/70 mix of non- and semi-volatile species. Higher volatility condensing vapors enable simulated growth of the nascent particles at a slower rate (relative to larger particles) than lower volatility condensing vapors. As a result, the newly formed particles grow more slowly with semi-volatile Arctic MSOA, which lowers the condensation and coagulation sinks (relative to non-volatile Arctic MSOA), and increases the total number of particles. As well, there is

relatively more condensation of the semi-volatile Arctic MSOA to larger particles, which contribute proportionately less to surface area and more to aerosol mass. These larger particles are efficiently removed by the frequent low-cloud drizzle of the summertime Arctic in our simulations. As shown on Fig. 2, the net effect is an increase in the number of ultrafine particles that better matches the observed time series of total number concentration.

3.3 Moments of the aerosol size distribution for Alert, Eureka and ship track

Figures 3, 4 and 5 show the 2016 summertime (July and August) median aerosol size distributions from SMPS measurements at Alert (Fig. 3), Eureka (Fig. 4), and for the 2016 ship track (Fig. 5). The figure panels show the zeroth through third moments of the aerosol size distribution, aerosol number, integrated diameter (length), surface area and volume. We define the aerosol number distribution (zeroth moment) as

$$n_N(D_p) = \frac{dN}{dlog_{10}D_p}. \tag{3}$$

The aerosol integrated diameter (length) distribution (first moment) is

$$n_D(D_p) = \frac{dD}{dlog_{10}D_p} = D\frac{dN}{dlog_{10}D_p}. \tag{4}$$

The aerosol surface area (second moment) is

$$n_S(D_p) = \frac{dS}{dlog_{10}D_p} = \pi D^2 \frac{dN}{dlog_{10}D_p}. \tag{5}$$

The aerosol volume (third moment) is

$$n_V(D_p) = \frac{dV}{dlog_{10}D_p} = \frac{\pi}{6}D^3\frac{dN}{dlog_{10}D_p}. \tag{6}$$

Atmos. Chem. Phys. Discuss., https://doi.org/10.5194/acp-2018-895
Manuscript under review for journal Atmos. Chem. Phys.
Discussion started: 18 September 2018

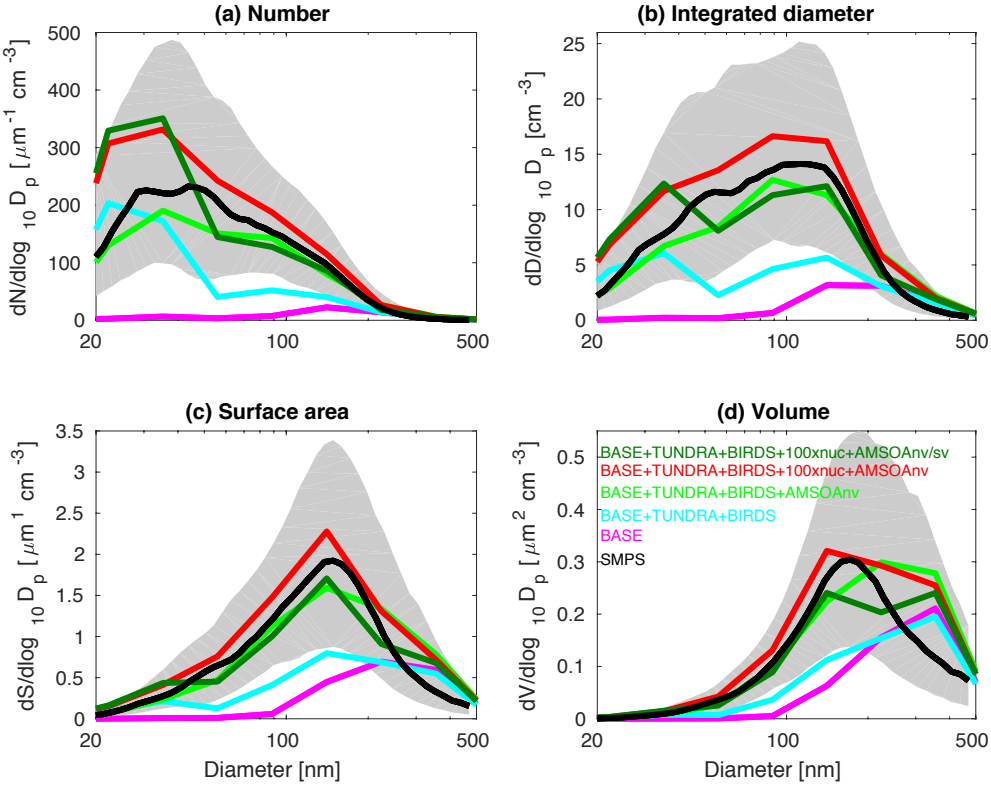

Figure 3: July and August 2016 median aerosol size distributions from scanning mobility particle sizer (SMPS) measurements at Alert (82.5° N, 62.3° W) (black) (described in Sect. 2.1) and for five GEOS-Chem-TOMAS simulations (color coded as shown on legend). Grey shading shows SMPS 20th to 80th percentile. Simulations are described in Table 1 and Sect. 2.3. Panels show aerosol distribution moments (a) aerosol number, (b) integrated aerosol diameter, (c) aerosol surface area, and (d) aerosol volume distributions. Note the different vertical scale relative to Figs. 4 and 5.

The observed distributions are similar between the three measurement sets. The number distributions peak in the Aitken mode at the particle diameter of 30-50 nm, which is

Atmos. Chem. Phys. Discuss., https://doi.org/10.5194/acp-2018-895
Manuscript under review for journal Atmos. Chem. Phys.
Discussion started: 18 September 2018

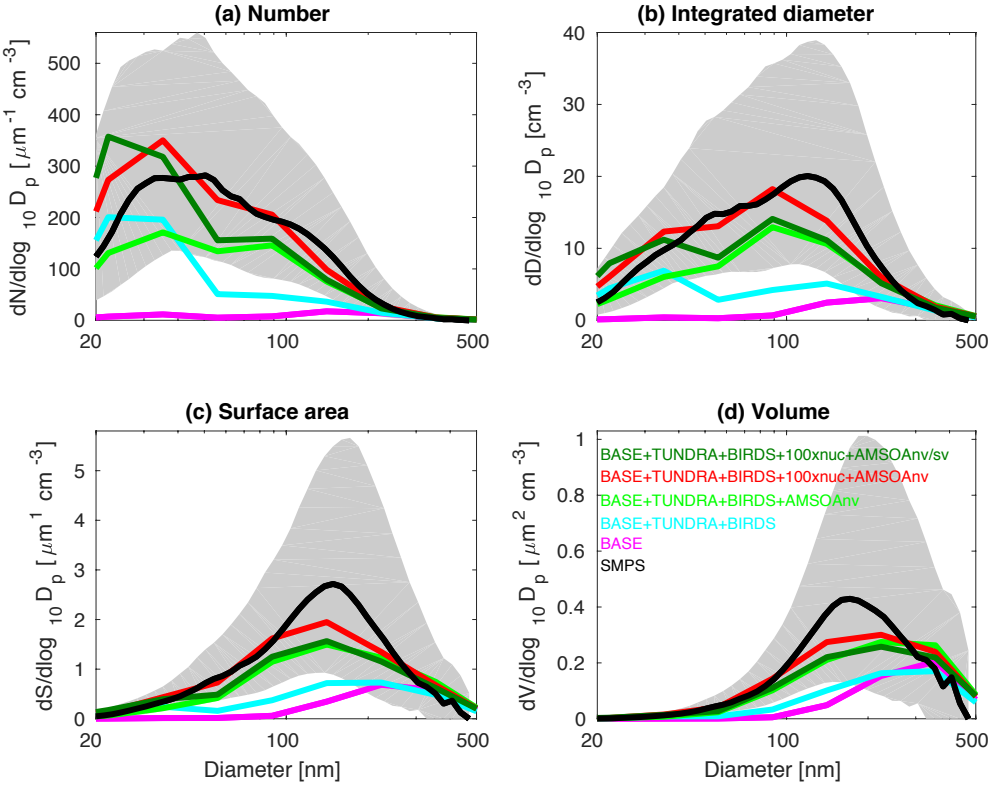

Figure 4: July and August 2016 median aerosol size distributions from scanning mobility particle sizer (SMPS) measurements at Eureka (80.1° N, 86.4° W) (black) (described in Sect. 2.1) and for five GEOS-Chem-TOMAS simulations (color coded as shown on legend). Grey shading shows SMPS 20th to 80th percentile. Simulations are described in Table 1 and Sect. 2.3. Panels show aerosol distribution moments (a) aerosol number, (b) integrated aerosol diameter, (c) aerosol surface area, and (d) aerosol volume distributions. Note the different vertical scale relative to Figs. 3 and 5.

similar to summertime observations at other pan-Arctic sites (Tunved et al., 2013; Asmi et al., 2016; Nguyen et al., 2016; Freud et al., 2017; Gunsch et al., 2017; Heintzenberg et al., 2017; Kolesar et al., 2017) and also in the central Arctic marine boundary layer (Heintzenberg and Leck, 2012; Karl et al., 2013; Heintzenberg et al., 2015). Interestingly, the value for the mode for the number distributions (dN/dlogD_p) has its smallest magnitude of about 200 cm^{-3} at the most northerly site (Alert), and increases moving southward to about 300 cm^{-3} at Eureka and 400 cm^{-3} for the ship track, which includes the

Atmos. Chem. Phys. Discuss., https://doi.org/10.5194/acp-2018-895
Manuscript under review for journal Atmos. Chem. Phys.
Discussion started: 18 September 2018

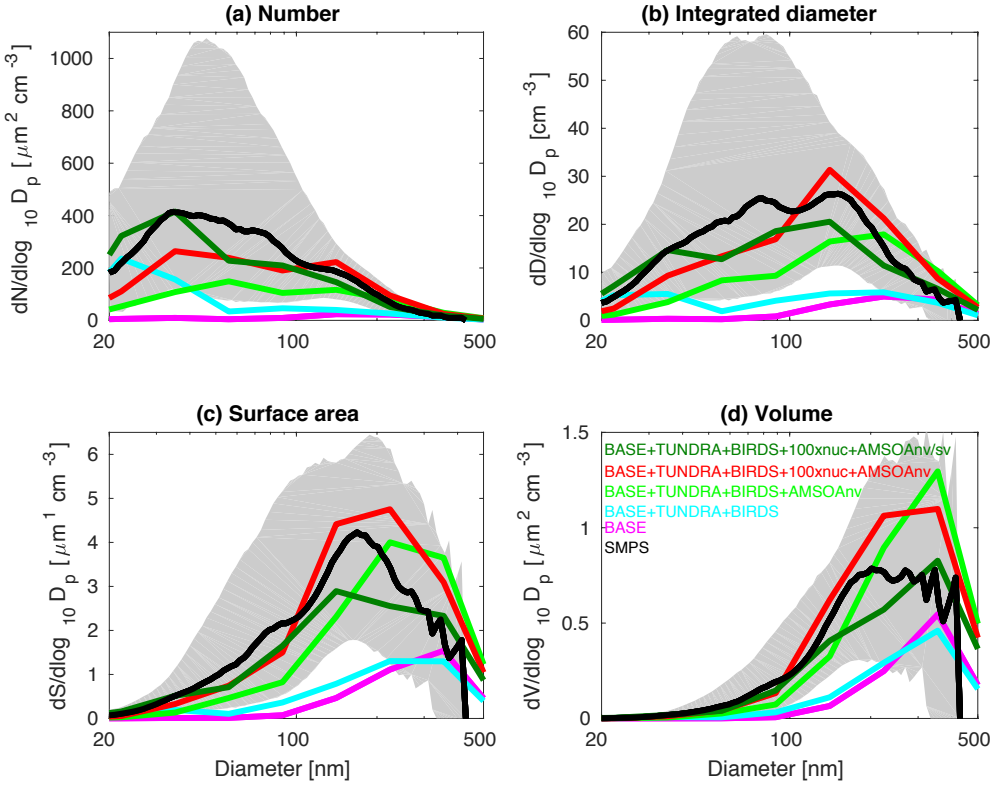

Figure 5: July and August 2016 median aerosol size distributions from scanning mobility particle sizer (SMPS) measurements for the *CCGS Amundsen* 2016 ship track (black) (described in Sect. 2.1) and for five GEOS-Chem-TOMAS simulations (color coded as shown on legend). Grey shading shows SMPS 20th to 80th percentile. Simulations are described in Table 1 and Sect. 2.3. Panels show aerosol distribution moments (a) aerosol number, (b) integrated aerosol diameter, (c) aerosol surface area, and (d) aerosol volume distributions. Note the different vertical scale relative to Figs. 3 and 4.

most southward extent. This pattern is consistent with the hypothesis of an important role for open water in building summertime aerosol size distributions (Heintzenberg et al., 2015; Willis et al., 2017; Dall´Osto et al., 2018b). A similar pattern is noted for the other three moments of the aerosol distribution.

Figures 3, 4 and 5 also show the simulated moments for the 3 sets of aerosol distributions. Simulation BASE strongly underpredicts all four moments of the distribution relative to all three of the measurement sets. Table 3 shows the MFE (Eq. (2))

between the simulations and measurements, using integrated values from the 4 moments of the distributions, similar to the approach employed by Hodshire et al. (2018). The MFEs are 1.17, 1.36 and 1.34 for Alert, Eureka, and the ship track, respectively, for simulation BASE. Implementation of sources of NH_3 from seabird-colonies (simulation BASE+BIRDS) reduces the MFE for all sites, and additional NH_3 from a tundra source for simulation BASE+TUNDRA+BIRDS further lowers the MFE at all sites (0.53 for Alert, 0.80 for Eureka and 0.97 for the ship track).

Mean Fractional Error	**Ship**	**Eureka**	**Alert**	**3-site mean**
BASE	1.34	1.36	1.17	1.29
Extra Ammonia				
BASE+BIRDS	1.16	1.13	0.75	1.01
BASE+TUNDRA	1.01	0.86	0.66	0.84
BASE+TUNDRA+BIRDS	0.97	0.80	0.53	0.77
Arctic MSOA (non-volatile)				
BASE+TUNDRA+BIRDS+AMSOAnv	0.43	0.35	0.13	0.30
Extra Nucleation				
BASE+TUNDRA+BIRDS+100xnuc	0.78	0.30	0.31	0.46
BASE+TUNDRA+BIRDS+100xnuc+AMSOAnv	0.22	0.08	0.30	0.20
Arctic MSOA volatility (mix non-/semi-volatile)				
BASE+TUNDRA+BIRDS+100xnuc+AMSOAnv/sv	0.11	0.24	0.10	0.15
BASE+TUNDRA+BIRDS+100xnuc+2xAMSOAnv/sv	0.22	0.09	0.27	0.19

Table 3: Mean fractional error (MFE) (Eq. (2)) between the nine GEOS-Chem-TOMAS simulations (described in Table 1 and Sect. 2.3) and the SMPS measurements (described in Sect. 2.1) for summertime- (July and August 2016) median aerosol size distributions at Alert, Eureka and during the *CCGS Amundsen* cruise shown in Figs. 3, 4, and 5, respectively.

Figures 3-5 also show that with the NH_3 from seabird colonies and tundra (simulation BASE+TUNDRA+BIRDS), an Aiken mode peak develops around 20-30 nm, but there is an underprediction of the number of aerosols with diameters between 30 nm to 200 nm and a strong underprediction of the aerosol diameter, surface area and volume moments. Simulation BASE+TUNDRA+BIRDS also underpredicts the organic carbon mass concentrations as shown in Table 2. This simulation suggests that condensation of H_2SO_4 and MSA alone do not yield sufficient particle growth to match observations from the Canadian Arctic Archipelago, which show frequent particle growth events (Willis et al., 2016; Collins et al., 2017; Burkart et al., 2017b; Tremblay et al., 2018) and suggest a key

role for growth by organic vapor condensation (Burkart et al., 2017a; Willis et al., 2017; Mungall et al., 2017). Marine primary organic aerosols could contribute to the Aitken mode as investigated further in the following Sect. 3.5.

With the implementation of Arctic MSOA (simulation BASE+TUNDRA+BIRDS+AMSOAnv), all four moments of the simulated aerosol distributions are more consistent with the measurements. The MFE is reduced for the ship track (0.43), Eureka (0.35) and Alert (0.13). These additional vapors condense on the simulated particles and build the aerosol diameter, surface area, and volume distributions to better represent the observations. For the ship track and at Eureka, scaling up the nucleation rate further reduces the MFE (simulation BASE+TUNDRA+BIRDS+100xnuc+AMSOAnv) by maintaining the number of ultrafine particles despite the increase in the condensation sink that arises with the growth from the Arctic MSOA. This scaling acts as a surrogate for nucleating vapors that could be missing in our simulations such as iodine (Allan et al., 2015; Dall´Osto et al., 2018a) and amines (Almeida et al., 2013), and also possible contribution from primary particle fragmentation (Leck and Bigg, 2010). For Alert, the MFE deteriorates with nucleation scaling suggesting that the standard ternary scheme yields sufficient particle formation for that portion of the Canadian Arctic Archipelago under the assumption of growth by non-volatile vapors.

The simulation with a 30/70 mix of non- and semi-volatile Arctic MSOA, respectively, (simulation BASE+TUNDRA+BIRDS+100xnuc+AMSOAnv/sv) yielded the lowest MFE for the ship track (0.11) and for Alert (0.10). We find a similarly low MFE for Eureka (0.09) with a doubling of the Arctic MSOA source under the assumption of a 30/70 mixed volatility (simulation BASE+TUNDRA+BIRDS+100xnuc+2xAMSOAnv/sv). Given that our simulations employ a fixed flux of Arctic MSOA-precursor vapors, and there is likely spatial variability in their source flux and oxidative aging to become available for condensation that is not well captured in our simulations; these intra-regional differences in the flux strength required to match observations are expected. For the same reasons, the

simulations do not perfectly capture the increase in the magnitude of the mode for the number, diameter, area and volume distributions between Alert and Eureka. However, simulation BASE+TUNDRA+BIRDS+100xnuc+AMSOAnv/sv (having lowest 3-site-mean MFE) does capture the larger magnitude of the mode value for all four moments for the ship track relative to those for Alert and Eureka.

Our finding that a mixture of non- and semi-volatile Arctic MSOA gives a closer fit between the simulations and observations is in agreement with the measurement-based findings of Burkart et al. (2017a) that the condensing vapors were surprisingly more volatile than at lower latitudes. As discussed by Burkart et al. (2017a), these semi-volatile (as opposed to non-volatile) vapors enable slower growth of the smallest mode of particles with diameters around 20 nm and faster growth of the larger mode with diameters around 90 nm. This larger mode is more efficiently removed by precipitation, maintaining a relatively pristine environment with lower particle mass concentrations that favors particle formation and growth.

The general improvements of the simulations with the addition of Arctic MSOA offers support for a key role of marine biogenic emissions in shaping the Arctic size distributions. Simulation BASE+TUNDRA+BIRDS+100xnuc+AMSOAnv/sv, specifically, yielded the lowest MFE for the total number concentration time series comparisons (Fig. 2), and had close agreement with the observed summertime mean organic carbon mass concentration at Alert (within about 10%, Table 2). As discussed in Sect. 3.1, several uncertainties affect the interpretation of the model-measurement comparisons for the quartz filter OC mass concentrations. The model-measurement fractional bias (FB) for the volume distribution (Table 4) provides a year-matched constraint on the total aerosol mass concentrations in our simulations without the complications associated with the quartz filter measurements such as the possibility of VOC uptake on the filters. Simulation BASE+TUNDRA+BIRDS+100xnuc+AMSOAnv/sv has the lowest volume distribution FB for both Alert (+0.07) and the ship track (+0.01), while for Eureka two simulations had the lowest FB, BASE+TUNDRA+BIRDS+100xnuc+AMSOAnv (-0.06) and

BASE+TUNDRA+BIRDS+100xnuc+2xAMSOAnv/sv (+0.06). For all three sites, implementation of Arctic MSOA reduced the fractional bias for the volume distribution relative to an otherwise similar simulation without Arctic MSOA. As shown in Table 2, all simulations generally matched the mass of sulfate+ammonium+MSA (and contributions of other measured species, e.g. nitrate, were minor) so organic aerosol is likely the most uncertain species.

Fractional Bias	**Ship**	**Eureka**	**Alert**
Base	-0.83	-0.87	-0.54
Extra Ammonia			
BASE+BIRDS	-0.83	-0.84	-0.50
BASE+TUNDRA	-0.84	-0.79	-0.45
BASE+TUNDRA+BIRDS	-0.79	-0.74	-0.38
Arctic MSOA (non-volatile)			
BASE+TUNDRA+BIRDS+AMSOAnv	+0.25	-0.20	+0.19
Extra Nucleation			
BASE+TUNDRA+BIRDS+100xnuc	-0.75	-0.69	-0.32
BASE+TUNDRA+BIRDS+100xnuc+AMSOAnv	+0.36	-0.06	+0.31
Arctic MSOA Volatility (mix non-/semi-volatile)			
BASE+TUNDRA+BIRDS+100xnuc+AMSOAnv/sv	+0.01	-0.22	+0.07
BASE+TUNDRA+BIRDS+100xnuc+2xAMSOAnv/sv	+0.38	+0.06	+0.38

Table 4: Fractional bias (as defined in Sect. 2.3) between the nine GEOS-Chem-TOMAS simulations (described in Table 1 and Sect. 2.3) and the SMPS volume distribution measurements (described in Sect. 2.1) for summertime- (July and August 2016) median aerosol size distributions at Alert, Eureka and during the *CCGS Amundsen* cruise shown in panel (d) on Figs. 3, 4, and 5, respectively

3.4 Role of Arctic MSOA during a growth event in Canadian Arctic Archipelago

Figure 6 provides an example of a particle growth event from the summer 2016 *CCGS Amundsen* ship track through the Canadian Arctic Archipelago. The observations during 14-15 August 2016 show growth of particles from about 15 nm to about 35 nm over a period of about 10 hours. Collins et al., 2017 and Burkart et al. (2017a) also report growth rates of about 2-4 nm h^{-1} for similar size aerosols during other growth events observed from the *CCGS Amundsen* during the 2016 cruise. The top right panel shows

Atmos. Chem. Phys. Discuss., https://doi.org/10.5194/acp-2018-895
Manuscript under review for journal Atmos. Chem. Phys.
Discussion started: 18 September 2018

that without the source of Arctic MSOA (simulation BASE+TUNDRA+BIRDS+100xnuc), the nascent particles do not exhibit sufficient growth beyond about 15 nm by condensation of H_2SO_4 and MSA alone. The bottom left panel shows that with the source of non-volatile

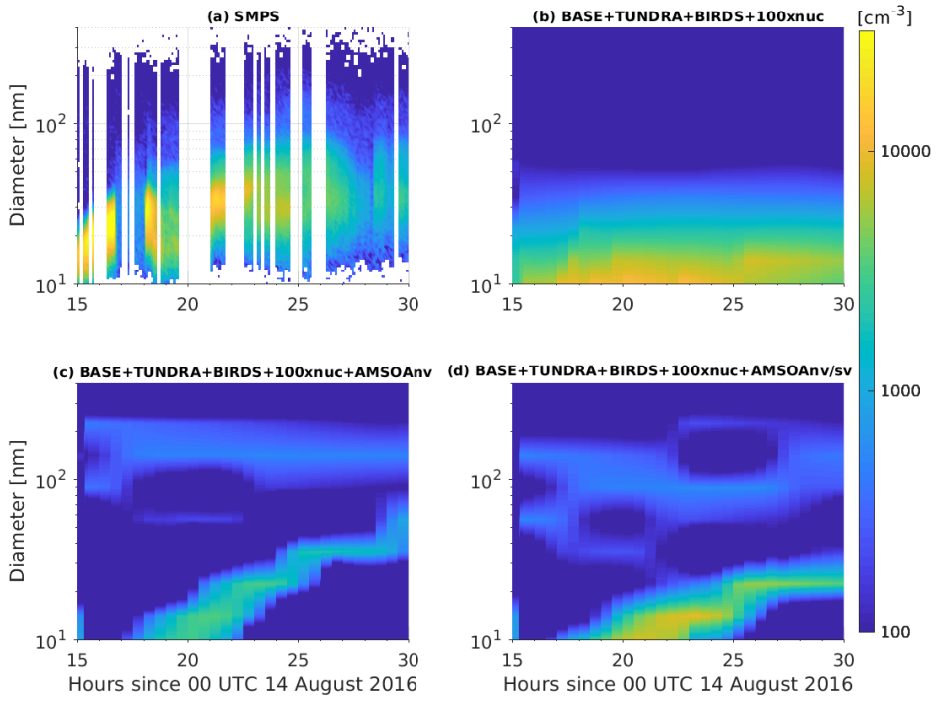

Figure 6: Time series of size-resolved aerosol number distributions (color contours show dN/dlogD$_p$) for the growth event of 14-15 August 2016 as (a) observed along the Amundsen ship track (described in Sect. 2.1) and for the GEOS-Chem-TOMAS simulations along the ship track (b) BASE+TUNDRA+BIRDS+100xnuc, (c) BASE+TUNDRA+BIRDS+100xnuc+AMSOAnv and (d) BASE+TUNDRA+BIRDS+100xnuc+AMSOAnv/sv. Simulations are described in Table 1 and Sect. 2.3.

Arctic MSOA for simulation BASE+TUNDRA+BIRDS+100xnuc+AMSOAnv, there is growth from about 10 nm to about 50 nm over 10 hours, a growth rate that is faster than observed for this event and faster than reported by Burkart et al., 2017a.

The bottom right panel of Fig. 6 shows for simulation BASE+TUNDRA+BIRDS+100xnuc+AMSOAnv/sv, particles grow from about 10 nm to

20 nm over about 8 hours, which is closer to the observed rate and slower than the simulation BASE+TUNDRA+BIRDS+100xnuc+AMSOAnv, which assumed non-volatile Arctic MSOA. Semi-volatile Arctic MSOA also enables faster growth of the larger mode around 90 nm, in agreement with the observations of Burkart et al. (2017a) that the larger mode grew faster. We note that the timing of the simulated event shown in Fig. 6 is not a perfect match to the observations. Capture of the timing of individual growth events is challenging for global models since sub-grid scale effects, including spatial variations in the meteorological fields over the time frame of few hours, such as cloud cover are not perfectly captured for the measurement site by the model resolution. However, similar to our findings from the previous sections, a source of mixed non- and semi-volatile Arctic MSOA also yields closer agreement with these measurements from the Canadian Arctic Archipelago during the summer of 2016. This key role for semi-volatile Arctic MSOA during the frequent summertime growth events in the Canadian Arctic Archipelago is consistent with measurement-based studies for this region (Willis et al., 2017; Collins et al., 2017; Burkart et al., 2017a; Leaitch et al., 2018; Tremblay et al., 2018).

3.5 Size-resolved aerosol composition

Few measurements are available of the composition of the summertime Arctic Aitken mode due to insufficient instrument detection limits to detect the extremely low mass concentrations in this size range (less than 100 ng m^{-3}). However the limited information available does provide insight into the processes that shape the size distribution. For example, Giamarelou et al. (2016) found that sub-12 nm particles in the Svalbard region were primarily ammoniated sulfates, pointing to the importance of particle formation by ternary nucleation of gas-phase NH_3, H_2SO_4 and water and initial growth by lower volatility sulfur-containing vapors.

Figure 7 shows the size-resolved mass fractions for the various aerosol components for simulation BASE+TUNDRA+BIRDS+100xnuc+AMSOAnv/sv. For the simulated sub-10 nm particles, the simulated summertime (July and August) mean mass fractions at

Alert, Eureka and for the ship track are primarily biogenic sulfate and MSA, which arise from oxidation of DMS, which is released to the atmosphere by marine biological activity. Thus, the simulated composition exhibits similarities with the Svalbard measurements, with the additional identification of a biogenic source. Figure 7 is also consistent with the strong summertime biogenic sulfate component observed in the Canadian Arctic Archipelago by Ghahremaninezhad et al. (2016).

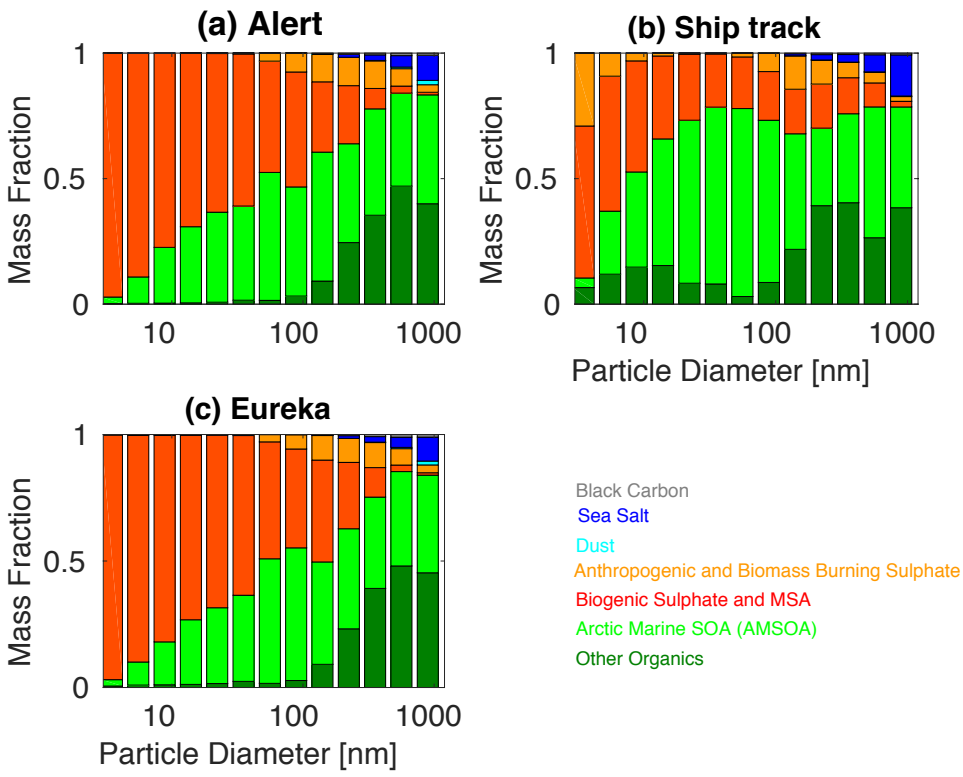

Figure 7: Simulated summertime- (July and August 2016) mean size-resolved aerosol component mass fractions for (a) Alert, (b) Amundsen ship track and (c) Eureka, for the simulation BASE+TUNDRA+BIRDS+100xnuc+AMSOAnv/sv as described in Table 1 and Sect. 2.3. Other organics includes all organic aerosol except the Arctic marine secondary organic aerosol (AMSOA). Biogenic sulfate includes all sulfate derived from the oxidation of dimethyl sulfide (DMS).

Limited measurements of the composition of particles with diameters between 60 to 100 nm during growth events at Eureka show that these particles are almost entirely composed of organic compounds, which could also include a minor contribution from MSA (Tremblay et al., 2018). Unfortunately, these measurements were limited to a few growth events and cannot be directly compared with the simulated summertime mean mass fractions shown in Fig. 7. Burkart et al. (2017a) calculated a cloud condensation nuclei (CCN) hygroscopicity parameter (Petters and Kreidenweis, 2007) for the particles during a growth event in the Canadian Arctic Archipelago and found a value also indicating a mostly organic composition for those particles large enough to act as CCN. Figure 7 shows that our simulation captures an increasing contribution of organics with particle diameters towards 50-100 nm (sizes that can act as CCN), reflecting the key role of organics in growth of particles towards sizes that can be climate-relevant by acting as seeds for cloud droplet formation, or directly scattering and absorbing radiation (diameters larger than about 100 nm). Semi-volatile organic vapors have also been shown to have a role in growth of particles after they reach diameters of about 5 nm (Tröstl et al., 2016). However, as noted by Karl et al. (2013) lower volatility vapors are needed for initial growth over the first few nm. Thus, semi-volatile organic vapors are likely only important in later growth beyond 10-20 nm.

Figure 7 shows that the simulated contribution of organics is greatest for the ship track, reflecting the marine source of the condensable organics in our simulation. The ship track also has the strongest contribution of 'other organics' in the sub-100 nm range, with a peak contribution for particle diameters of 10-30 nm. This sub-100 nm organic contribution (shaded in dark green on Fig. 7) represents the mass-fraction contribution of primary marine organics in our simulation. These primary particles also grow to larger sizes by condensation of Arctic MSOA in our simulations. As described in Sect. 2.2, all sea spray emissions with diameters smaller than 100 nm are treated as hydrophobic organic carbon. We use the Mårtensson et al. (2003) parameterization, which can be considered as the upper limit of sea spray emissions for the sub-100 nm range, relative to other parameterizations. As a result, we consider that our simulation provides an upper limit on the mass fraction of marine primary organic aerosol in the Aitken mode in the

Canadian Arctic Archipelago region. The primary aerosol, particularly in the marine boundary layer, is climate-relevant as it grows by condensation of Arctic MSOA towards sizes of 50 nm to 100 nm. The dark green shading ('other organics') on Fig. 7 for sizes larger than 100 nm represents contributions to the mass fractions by organics that have been transported from lower latitudes, including those primary and secondary aerosols from biomass burning and other non-marine lower-latitude sources.

3.6 Impact of Arctic MSOA on climate-relevant aerosol number concentrations, direct and indirect radiative effects

In this section, we consider the role of Arctic MSOA on the simulated total number concentration of aerosols with diameter larger than 50 nm (N50) and 100 nm (N100) and the associated radiative effects using our simulation with the lowest overall model-measurement MFE (simulation BASE+TUNDRA+BIRDS+100xnuc+AMSOAnv/sv) relative to the simulation without Arctic MSOA (BASE+TUNDRA+BIRDS+100xnuc). Figure 8 shows the pan-Arctic distribution of the simulated summertime- (July and August) mean surface-layer N50 and N100 for simulation BASE+TUNDRA+BIRDS+100xnuc+AMSOAnv/sv. In the Canadian Arctic Archipelago region, the simulated summertime-mean N50 (50 cm^{-3} to 100 cm^{-3}) and N100 (10 cm^{-3} to 30 cm^{-3}) ranges are consistent with monthly mean values from observations at Alert presented in Croft et al. (2016b). The panels in the middle column of Fig. 8 show that the addition of Arctic MSOA (simulation BASE+TUNDRA+BIRDS+100xnuc+AMSOAnv/sv relative to BASE+TUNDRA+BIRDS+100xnuc) yields a N50 increase of about 50-75 cm^{-3} and a N100 increase of about 20 cm^{-3} in the Canadian Arctic Archipelago. These differences in the simulated N50 and N100 are attributed to the process of growth by condensation of Arctic MSOA, and will have climate-relevant impacts on aerosol radiative effects.

Atmos. Chem. Phys. Discuss., https://doi.org/10.5194/acp-2018-895
Manuscript under review for journal Atmos. Chem. Phys.
Discussion started: 18 September 2018

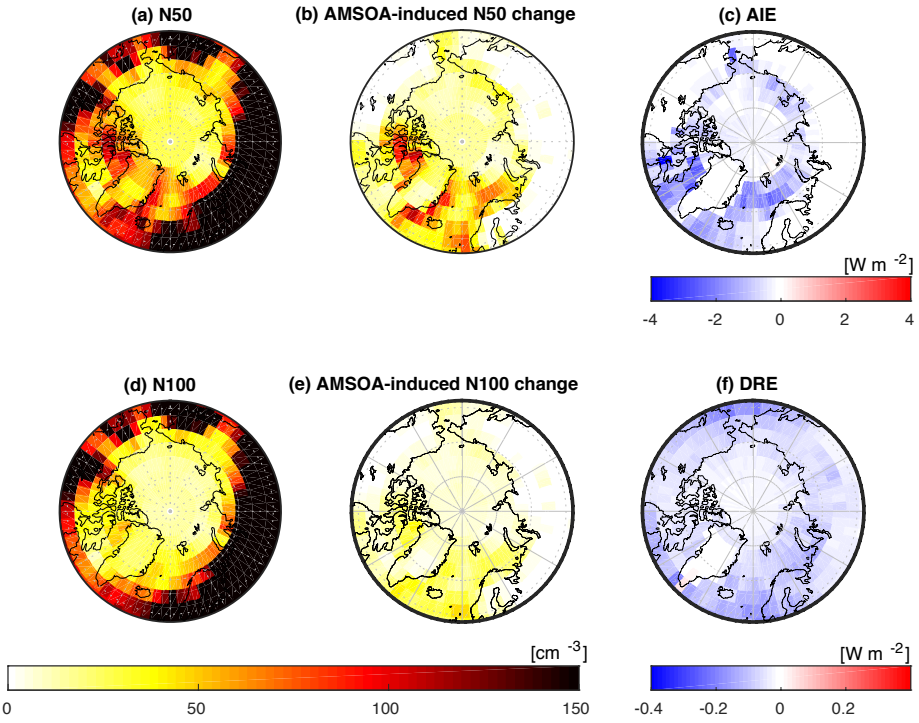

Figure 8: Impact of Arctic MOSA, simulated summertime- (July and August 2016) mean geographic distribution of surface-layer aerosol number concentrations for (a) particles with diameters larger than 50 nm (N50) for simulation BASE+TUNDRA+BIRDS+100xnuc+AMSOAnv/sv, (b) surface-layer N50 difference for simulation BASE+TUNDRA+BIRDS+100xnuc+AMSOAnv/sv relative to simulation BASE+TUNDRA+BIRDS+100xnuc, (c) aerosol indirect effect (AIE) at top of the atmosphere (methodology described in Sect. 2.2) between these two simulations, attributed to Arctic MSOA (AMSOA), (d) similar to a) but for N100, (e) similar to (b) but for N100 difference, (f) direct aerosol effect (DRE) at top of the atmosphere (methodology described in Sect. 2.2) between these two simulations, attributed to Arctic MSOA (AMSOA).

Figure 8 also shows the geographic distribution of the top-of-the-atmosphere DRE and cloud-albedo AIE (described in Sect. 2.2) for marine SOA (comparing between simulations BASE+TUNDRA+BIRDS+100xnuc and BASE+TUNDRA+BIRDS+100xnuc+AMSOAnv/sv). The pan-Arctic mean DRE attributed to condensational growth by Arctic MSOA is -0.04 W m^{-2}. The simulated Arctic MSOA effect is largest (about –0.1 W m^{-2} to -0.2 W m^{-2}) over the regions of open water such as Baffin Bay, east of Greenland, and the Bering Sea. These are also regions

of the largest N100 change since those particles with diameters larger than about 100 nm contribute strongly to scattering of solar radiation. Although our simulated Arctic MSOA-precursor vapor flux yielded particle distributions that were in close agreement with observations from the Canadian Arctic Archipelago (as shown in previous sections), there is considerable uncertainty about the Arctic MSOA source function such that terrestrial sources could also be missing from our simulations. These effects could change the spatial distribution and magnitude of the DRE. Further work is needed to better understand the source and nature of Arctic MSOA-precursor vapors in the Arctic to reduce uncertainties in the associated DRE.

The pan-Arctic mean cloud-albedo AIE attributed to Arctic MSOA is about -0.4 W m^{-2}. The AIE shows a similar geographic distribution to the changes in the N50, with largest values of -1 to -2 W m^{-2} in the Canadian Arctic Archipelago and east of Greenland, again related to the open water regions associated with the Arctic MSOA-precursor vapor flux implemented in our simulations. As with the DRE, there is a large uncertainty associated with the spatial distribution of this AIE due to the uncertainty about the source function for Arctic MSOA. However, we view this calculation as an indication that the impact of condensational growth by Arctic MSOA is expected to be relevant for the Arctic climate. Work is needed to better understand the composition and source flux of Arctic MSOA-precursor vapors.

4. Conclusions

We used the GEOS-Chem-TOMAS chemical transport model with size-resolved aerosol microphysics to interpret measurements conducted during the summertime of 2016 in the Canadian Arctic Archipelago, some as part of the NETwork on Climate and Aerosols: addressing key uncertainties in Remote Canadian Environments (NETCARE) project (Abbatt et al. (in prep.)). Three measurement platforms were considered. These platforms were located at Alert and Eureka, both in Nunavut, Canada and also onboard the *CCGS Amundsen*. We focused on examining the key processes that build summertime aerosol size distributions in this region, particularly the role of Arctic marine secondary organic

aerosol (Arctic MSOA) condensation. The terminology Arctic MSOA was used to indicate secondary organic aerosol formed from precursors from marine (open ocean and coastal) sources north of 50° N, excluding MSA, which we treated as a separate aerosol component. In the Canadian Arctic Archipelago, Arctic MSOA is likely strongly controlled by emissions from marine biogenic activity (Willis et al., 2017; Leaitch et al. 2018).

We find that Arctic MSOA contributes strongly to the summertime particle size distributions in the Canadian Arctic Archipelago. Building on measurement-based studies from the NETCARE project, we implemented a flux of condensable Arctic MSOA-precursor vapors into our GEOS-Chem-TOMAS simulations. This fixed flux of 500 μg m^{-2} d^{-1} of Arctic MSOA-precursor vapors (with a yield of unity) emitted from open seawater in the Arctic and near Arctic (north of 50° N) was a crude representation of the source function because of the lack of knowledge about the nature and source of Arctic MSOA. However, implementation of condensable Arctic MSOA in our simulation reduced the model-to-measurement MFE for the summertime median aerosol size distributions by a factor of 2-4 across the three measurement platforms, indicating a strong sensitivity of the simulated size distributions to growth by Arctic MSOA. Without Arctic MSOA, particle growth to diameters of 50 nm to 200 nm was strongly underpredicted in our simulations. Increasing the particle nucleation rate by 100-fold further reduced the MFE for Eureka and the ship track, indicating that additional materials such as (but not limited to) gas-phase iodine, and/or amines and/or possibly extremely low volatility organics may be participating in nucleation, and/or other mechanisms such as particle fragmentation, leading to faster rates than our ternary scheme.

Introduction of a 30/70 non-/semi-volatile split for the simulated Arctic MSOA reduced by 2- to 3-fold the model-to-measurement MFE for the summertime aerosol size distributions for Alert (0.10) and the ship track (0.10), and also yielded the lowest MFE for Eureka (0.09) if the Arctic MSOA-precursor vapor source flux was doubled. These findings offer support that the condensing Arctic MSOAs contributing to growth of

particles with diameters larger than about 20 nm in the Canadian Arctic Archipelago could contain a large fraction of semi-volatile species.

Size-resolved mass fractions indicated that initial growth of simulated nascent sub-10 nm particles (arising from ternary nucleation of ammonia sulfuric acid, water vapors) occurred primarily by condensation involving biogenic sulfate and MSA, both derived from oxidation of dimethyl sulfide of marine origin. Arctic MSOA contributed about 20-80% to size-resolved particle mass for diameters between 10 nm and 100 nm, with the largest contributions for the ship track simulation. The simulated contribution of primary organics of sea-spray origin to sub-100 nm particle mass fractions was largest for the ship track simulation in the marine boundary layer, with mass fractions approaching 20% for particles with diameters around 10 nm to 20 nm.

By comparing our best (lowest MFE) simulations with and without the Arctic MSOA formed from precursors with marine sources north of 50° N, we found that Arctic MSOA had a strong summertime- and pan-Arctic-mean top-of-the-atmosphere aerosol direct radiative effect (DRE) of -0.04 W m^{-2}, and cloud-albedo aerosol indirect effect (AIE) of -0.4 W m^{-2}. The comparison of these simulations with and without Arctic MSOA suggested a strong sensitivity of climate-relevant effects to Arctic MSOA. However, we caution that a high level of uncertainty is associated with our quantification of these effects, due to uncertainty about the composition, and source fluxes for these condensing vapors. Future studies are needed to reduce these uncertainties.

Many knowledge gaps remain regarding the role of organics within the processes that shape particle size distributions in the Arctic climate system. For example, Willis et al. (2017) found that the organics in the aerosol in the summertime Canadian Arctic Archipelago were not like typical biogenic SOA, having instead a character with a long hydrocarbon chain, implying a fatty-acid-type precursor, which is a common component of the marine microlayer. Additionally, Mungall et al. (2017) found that the marine microlayer in the Canadian Arctic Archipelago was a source of OVOCs, which could also be related to Arctic MSOA. Further measurements are needed to identify the organic

vapors that yield Arctic MSOA through condensational particle growth, along with their sources, chemistry, and spatial distribution within the Arctic. Additionally, given the climate relevance of NH_3 through formation of nascent particles, measurements are needed to better identify and quantify its sources across the summertime Arctic, and to further examine the spatial distribution of the subsequent Arctic particle growth events. Further, size-resolved particle concentrations and composition measurements (particularly for sulfate and organic aerosol), would constrain the controlling processes for all sub-micron particle diameters. Such work could also reduce uncertainty related to aerosol effects within the Arctic climate system. This work will also lay a foundation for prediction of future aerosol effects within the context of our rapidly changing and warming Arctic, as sea ice extent, biological and anthropogenic activity are altered.

Acknowledgements:

We thank the Observatory operators at Alert, Desiree Toom, Alina Chivulescu, Dan Veber, Wendy Zhang, Darrell Ernst as well as Andrew Platt and Carrie Taylor for their support of the Environment and Climate Change Canada (ECCC) aerosol programme at Alert and Eureka. We are grateful for the hard work and dedication of the *CCGS Amundsen* crew and for the help of our colleagues on board. We thank O. Kupiainen-Määttä, T. Olenius, J. Julin, H. Vehkamäki, B. Murphy, and I. Riipinen for their support of this project through provision of the Atmospheric Cluster Dynamics Code (ACDC). The authors also thank Bonne Ford and Katelyn O'Dell for preparing the 2016 GFED4 files in the format required for input to the GEOS-Chem-TOMAS model.

This work is supported by the Climate Change and Atmospheric Research programme at NSERC, as part of the NETCARE project. This work was also supported by Environment and Climate Change Canada (ECCC) and by the Ocean Frontier Institute. R. Chang, S. Tremblay and P. Hayes acknowledge support from the NSERC CCAR project Probing the Atmosphere of the High Arctic (PAHA) led by PI James R. Drummond as well as support from the NSERC Discovery Grant programme (RGPIN-05002-2014, RGPIN-05173-2014) and CANDAC (Canadian Network for the Detection of Atmospheric

Change). Colorado State University researchers were supported by the US Department of Energy's Atmospheric System Research, an Office of Science, Office of Biological and Environmental Research program, under Grant No. DE-SC0011780, the U.S. National Science Foundation, Atmospheric Chemistry program, under Grant No. AGS-1559607, and by the U.S National Oceanic and Atmospheric Administration, an Office of Science, Office of Atmospheric Chemistry, Carbon Cycle, and Climate Program, under the cooperative agreement award No. NA17OAR430001. A. Moravek's work was supported by the NSERC CREATE program IACPES postdoctoral fellowship.

References

Abbatt, J. P. D., Leaitch, W. R., Aliabadi, A. A., Bertram, A. K., Blanchet, J.-P., Bozem, H., Burkart, J., Chang, R., Chaubey, J.-P., Christensen, R. J., Cirisan, A., Collins, D. B., Croft, B., Dionne, J., Evans, G., Fletcher, C., Ghahremaninezhad, R,. Girard, E., Gong, W., Gosselin, M., Gourdal, M., Hanna, S., Hayashida, H., Herber, A., Hesaraki, S., Hoor, P., Huang, L., Hussherr, R., Irish, V. E., Keita, S., Kodros, J. K., Köllner, F., Kolonjari, F., Kunkel, D., Ladino, L. A., Law, K., Levasseur, M., Libois, Q., Liggio, J., Lizotte, M., Macdonald, K., Mahmood, R., Martin, R. V., Mason, R. H., Miller, L., Moravek, A., Mortenson, E., Mungall, E., Murphy, J. G., Namazi, M., Norman, A.-L., O'Neill, N., Pierce, J.R., Russell, L. M., Schneider, J., Schulz, H., Sharma, S., Si, M., Staebler, R. M., Steiner, N. S., Tapias, M., Thomas, J., von Salzen, K., Wentzell, J., Willis, M. D., Wentworth, G. R., Xu, J.-W., Yakobi-Hancock, J. D.: New insights into aerosol and climate in the Arctic (in prep.), 2018.

Abdul-Razzak, H.: A parameterization of aerosol activation 3. Sectional representation, J. Geophys. Res., 107(D3), 4026, doi:10.1029/2001JD000483, 2002.

Alexander, B., Allman, D. J., Amos, H. M., Fairlie, T. D., Dachs, J., Hegg, D. A. and Sletten, R. S.: Isotopic constraints on the formation pathways of sulfate aerosol in the marine boundary layer of the subtropical northeast Atlantic Ocean, J. Geophys. Res. Atmos., 117(6), 1–17, doi:10.1029/2011JD016773, 2012.

Allan, J. D., Williams, P. I., Najera, J., Whitehead, J. D., Flynn, M. J., Taylor, J. W., Liu, D., Darbyshire, E., Carpenter, L. J., Chance, R., Andrews, S. J., Hackenberg, S. C. and McFiggans, G.: Iodine observed in new particle formation events in the Arctic atmosphere during ACCACIA, Atmos. Chem. Phys., 15(10), 5599–5609, doi:10.5194/acp-15-5599-2015, 2015.

Almeida, J., Schobesberger, S., Kürten, A., Ortega, I. K., Kupiainen-Määttä, O., Praplan, A. P., Adamov, A., Amorim, A., Bianchi, F., Breitenlechner, M., David, A., Dommen, J., Donahue, N. M., Downard, A., Dunne, E., Duplissy, J., Ehrhart, S., Flagan, R. C., Franchin, A., Guida, R., Hakala, J., Hansel, A., Heinritzi, M., Henschel, H., Jokinen, T.,

Junninen, H., Kajos, M., Kangasluoma, J., Keskinen, H., Kupc, A., Kurtén, T., Kvashin, A. N., Laaksonen, A., Lehtipalo, K., Leiminger, M., Leppä, J., Loukonen, V., Makhmutov, V., Mathot, S., McGrath, M. J., Nieminen, T., Olenius, T., Onnela, A., Petäjä, T., Riccobono, F., Riipinen, I., Rissanen, M., Rondo, L., Ruuskanen, T., Santos, F. D., Sarnela, N., Schallhart, S., Schnitzhofer, R., Seinfeld, J. H., Simon, M., Sipilä, M., Stozhkov, Y., Stratmann, F., Tomé, A., Tröstl, J., Tsagkogeorgas, G., Vaattovaara, P., Viisanen, Y., Virtanen, A., Vrtala, A., Wagner, P. E., Weingartner, E., Wex, H., Williamson, C., Wimmer, D., Ye, P., Yli-Juuti, T., Carslaw, K. S., Kulmala, M., Curtius, J., Baltensperger, U., Worsnop, D. R., Vehkamäki, H. and Kirkby, J.: Molecular understanding of sulphuric acid-amine particle nucleation in the atmosphere, Nature, 502(7471), 359–363, doi:10.1038/nature12663, 2013.

Amos, H. M., Jacob, D. J., Holmes, C. D., Fisher, J. A., Wang, Q., Yantosca, R. M., Corbitt, E. S., Galarneau, E., Rutter, A. P., Gustin, M. S., Steffen, A., Schauer, J. J., Graydon, J. A., St Louis, V. L., Talbot, R. W., Edgerton, E. S., Zhang, Y. and Sunderland, E. M.: Gas-particle partitioning of atmospheric Hg(II) and its effect on global mercury deposition, Atmos. Chem. Phys., 12(1), 591–603, doi:10.5194/acp-12-591-2012, 2012.

Asmi, E., Kondratyev, V., Brus, D., Laurila, T., Lihavainen, H., Backman, J., Vakkari, V., Aurela, M., Hatakka, J., Viisanen, Y., Uttal, T., Ivakhov, V. and Makshtas, A.: Aerosol size distribution seasonal characteristics measured in Tiksi, Russian Arctic, Atmos. Chem. Phys., 16, 1271–1287, doi:10.5194/acp-16-1271-2016, 2016.

Baranizadeh, E., Murphy, N. B., Julin, J., Falahat, S., Reddington, L. C., Arola, A., Ahlm, L., Mikkonen, S., Fountoukis, C., Patoulias, D., Minikin, A., Hamburger, T., Laaksonen, A., Pandis, N. S., Vehkamäki, H., Lehtinen, E. J. K. and Riipinen, I.: Implementation of state-of-the-art ternary new-particle formation scheme to the regional chemical transport model PMCAMx-UF in Europe, Geosci. Model Dev., 9(8), 2741–2754, doi:10.5194/gmd-9-2741-2016, 2016.

Barnes, I., Hjorth, J. and Mihalopoulos, N.: Dimethyl Sulfide and Dimethyl Sulfoxide and Their Oxidation in theirAtmosphere, Chem. Rev., 106, 940–975, doi:10.1021/cr020529+, 2006.

Barrie, L. A.: Arctic Aerosols: Composition, Sources and Transport BT - Ice Core Studies of Global Biogeochemical Cycles, edited by R. J. Delmas, pp. 1–22, Springer Berlin Heidelberg, Berlin, Heidelberg., 1995.

Bond, T. C., Bhardwaj, E., Dong, R., Jogani, R., Jung, S., Roden, C., Streets, D. G. and Trautmann, N. M.: Historical emissions of black and organic carbon aerosol from energy-related combustion, 1850-2000, Global Biogeochem. Cycles, 21(2), 1–16, doi:10.1029/2006GB002840, 2007.

Bouwman, A. F., Lee, D. S., Asman, W. A. H., Dentener, F. J., Hoek, K. W. Van Der, Olivier, J. G. J. and Tg, N.: A global high-resolution emission inventory for ammonia,

Global Biogeochem. Cycles, 11(4), 561–587, 1997.

Boylan, J. W. and Russell, A. G.: PM and light extinction model performance metrics, goals, and criteria for three-dimensional air quality models, Atmos. Environ., 40(26), 4946–4959, doi:10.1016/j.atmosenv.2005.09.087, 2006.

Breider, T. J., Mickley, L. J., Jacob, D. J., Wang, Q. Q., Fisher, J. A., Chang, R. Y. and Alexander, B.: Annual distributions and sources of Arctic aerosol components, aerosol optical depth, and aerosol absorption, J. Geophys. Res. Atmos., 119, 4107–4124, doi:10.1002/2013JD020996, 2014.

Breider, T. J., Mickley, L. J., Jacob, D. J., Ge, C., Wang, J., Sulprizio, M. P., Croft, B., Ridley, D. A., Mcconnell, J. R., Sharma, S., Husain, L., Dutkiewicz, V. A., Eleftheriadis, K., Skov, H. and Hopke, P. K.: Multidecadal trends in aerosol radiative forcing over the Arctic: Contribution of changes in anthropogenic aerosol to Arctic warming since 1980, J. Geophys. Res. Atmos., 122, doi:10.1002/2016JD025321, 2017.

Brock, C. A., Cozic, J., Bahreini, R., Froyd, K. D., Middlebrook, A. M., McComiskey, A., Brioude, J., Cooper, O. R., Stohl, A., Aikin, K. C., De Gouw, J. A., Fahey, D. W., Ferrare, R. A., Gao, R. S., Gore, W., Holloway, J. S., Hübler, G., Jefferson, A., Lack, D. A., Lance, S., Moore, R. H., Murphy, D. M., Nenes, A., Novelli, P. C., Nowak, J. B., Ogren, J. A., Peischl, J., Pierce, R. B., Pilewskie, P., Quinn, P. K., Ryerson, T. B., Schmidt, K. S., Schwarz, J. P., Sodemann, H., Spackman, J. R., Stark, H., Thomson, D. S., Thornberry, T., Veres, P., Watts, L. A., Warneke, C. and Wollny, A. G.: Characteristics, sources, and transport of aerosols measured in spring 2008 during the aerosol, radiation, and cloud processes affecting Arctic Climate (ARCPAC) Project, Atmos. Chem. Phys., 11(6), 2423–2453, doi:10.5194/acp-11-2423-2011, 2011.

Browse, J., Carslaw, K. S., Arnold, S. R., Pringle, K. and Boucher, O.: The scavenging processes controlling the seasonal cycle in Arctic sulphate and black carbon aerosol, Atmos. Chem. Phys., 12(15), 6775–6798, doi:10.5194/acp-12-6775-2012, 2012.

Burkart, J., Hodshire, A. L., Mungall, E. L., Pierce, J. R., Collins, D. B., Ladino, L. A., Lee, A. K. Y., Irish, V., Wentzell, J. J. B., Liggio, J., Papakyriakou, T., Murphy, J. and Abbatt, J.: Organic Condensation and Particle Growth to CCN Sizes in the Summertime Marine Arctic Is Driven by Materials More Semivolatile Than at Continental Sites, Geophys. Res. Lett., 44(20), 10,725-10,734, doi:10.1002/2017GL075671, 2017a.

Burkart, J., Willis, M. D., Bozem, H., Thomas, J. L., Law, K., Hoor, P., Aliabadi, A. A., Köllner, F., Schneider, J., Herber, A., Abbatt, J. P. D. and Richard Leaitch, W.: Summertime observations of elevated levels of ultrafine particles in the high Arctic marine boundary layer, Atmos. Chem. Phys., 17(8), 5515–5535, doi:10.5194/acp-17-5515-2017, 2017b.

Carpenter, L. J. and Nightingale, P. D.: Chemistry and Release of Gases from the Surface Ocean, Chem. Rev., 115(10), 4015–4034, doi:10.1021/cr5007123, 2015.

Carpenter, L. J., Archer, S. D. and Beale, R.: Ocean-atmosphere trace gas exchange, Chem. Soc. Rev., 41(19), 6473–6506, doi:10.1039/c2cs35121h, 2012.

Carslaw, K. S., Lee, L. A., Reddington, C. L., Pringle, K. J., Rap, A., Forster, P. M., Mann, G. W., Spracklen, D. V, Woodhouse, M. T., Regayre, L. A. and Pierce, J. R.: Large contribution of natural aerosols to uncertainty in indirect forcing, Nature, 503, 67 [online] Available from: http://dx.doi.org/10.1038/nature12674, 2013.

Chang, R. Y. W., Leck, C., Graus, M., Müller, M., Paatero, J., Burkhart, J. F., Stohl, A., Orr, L. H., Hayden, K., Li, S. M., Hansel, A., Tjernström, M., Leaitch, W. R. and Abbatt, J. P. D.: Aerosol composition and sources in the central Arctic Ocean during ASCOS, Atmos. Chem. Phys., 11(20), 10619–10636, doi:10.5194/acp-11-10619-2011, 2011a.

Chang, R. Y. W., Sjostedt, S. J., Pierce, J. R., Papakyriakou, T. N., Scarratt, M. G., Michaud, S., Levasseur, M., Leaitch, W. R. and Abbatt, J. P. D.: Relating atmospheric and oceanic DMS levels to particle nucleation events in the Canadian Arctic, J. Geophys. Res. Atmos., 116(21), 1–10, doi:10.1029/2011JD015926, 2011b.

Charlson, R. J., Schwartz, S. E., Hales, J. M., Cess, R. D., Coakley, J. A., Hansen, J. E. and Hofmann, D. J.: Climate Forcing by Anthropogenic Aerosols, Science (80-.)., 255(5043), 423–430 [online] Available from: http://science.sciencemag.org/content/255/5043/423.abstract, 1992.

Chatfield, R. B. and Crutzen, P. J.: Are There Interactions of Iodine and Sulfur Species in Marine Air Photochemistry, J. Geophys. Res., 95(D13), 22319–22341, doi:10.1029/JD095iD13p22319, 1990.

Chin, M., Jacob, D. J., Gardner, G. M., Foreman-Fowler, M. S., Spiro, P. A. and Savoie, D. L.: A global three-dimensional model of tropospheric sulfate, J. Geophys. Res. Atmos., 101(D13), 18667–18690, doi:10.1029/96JD01221, 1996.

Chiu, R., Tinel, L., Gonzalez, L., Ciuraru, R., Bernard, F., George, C. and Volkamer, R.: UV photochemistry of carboxylic acids at the air-sea boundary: A relevant source of glyoxal and other oxygenated VOC in the marine atmosphere, Geophys. Res. Lett., 44(2), 1079–1087, doi:10.1002/2016GL071240, 2017.

Collins, D. B., Ault, A. P., Moffet, R. C., Ruppel, M. J., Cuadra-Rodriguez, L. A., Guasco, T. L., Corrigan, C. E., Pedler, B. E., Azam, F., Aluwihare, L. I., Bertram, T. H., Roberts, G. C., Grassian, V. H. and Prather, K. A.: Impact of marine biogeochemistry on the chemical mixing state and cloud forming ability of nascent sea spray aerosol, J. Geophys. Res. Atmos., 118(15), 8553–8565, doi:10.1002/jgrd.50598, 2013.

Collins, D. B., Bertram, T. H., Sultana, C. M., Lee, C., Axson, J. L. and Prather, K. A.: Phytoplankton blooms weakly influence the cloud forming ability of sea spray aerosol, Geophys. Res. Lett., 43(18), 9975–9983, doi:10.1002/2016GL069922, 2016.

Collins, D. B., Burkart, J., Chang, R. Y.-W., Lizotte, M., Boivin-Rioux, A., Blais, M., Mungall, E. L., Boyer, M., Irish, V. E., Massé, G., Kunkel, D., Tremblay, J.-É., Papakyriakou, T., Bertram, A. K., Bozem, H., Gosselin, M., Levasseur, M. and Abbatt, J. P. D.: Frequent Ultrafine Particle Formation and Growth in the Canadian Arctic Marine Environment, Atmos. Chem. Phys., 17, 13119-13138, doi:10.5194/acp-17-13119-2017, 2017.

Crippa, M., Janssens-Maenhout, G., Dentener, F., Guizzardi, D., Sindelarova, K., Muntean, M., Van Dingenen, R. and Granier, C.: Forty years of improvements in European air quality: Regional policy-industry interactions with global impacts, Atmos. Chem. Phys., 16(6), 3825–3841, doi:10.5194/acp-16-3825-2016, 2016.

Croft, B., Wentworth, G. R., Martin, R. V., Leaitch, W. R., Murphy, J. G., Murphy, B. N., Kodros, J. K., Abbatt, J. P. D. and Pierce, J. R.: Contribution of Arctic seabird-colony ammonia to atmospheric particles and cloud-albedo radiative effect, Nat. Commun., 7, 1–10, doi:10.1038/ncomms13444, 2016a.

Croft, B., Martin, R. V., Richard Leaitch, W., Tunved, P., Breider, T. J., D'Andrea, S. D. and Pierce, J. R.: Processes controlling the annual cycle of Arctic aerosol number and size distributions, Atmos. Chem. Phys., 16(6), 3665–3682, doi:10.5194/acp-16-3665-2016, 2016b.

D'Andrea, S. D., Häkkinen, S. A. K., Westervelt, D. M., Kuang, C., Levin, E. J. T., Kanawade, V. P., Leaitch, W. R., Spracklen, D. V., Riipinen, I. and Pierce, J. R.: Understanding global secondary organic aerosol amount and size-resolved condensational behavior, Atmos. Chem. Phys., 13(22), 11519–11534, doi:10.5194/acp-13-11519-2013, 2013.

Dall´Osto, M., Beddows, D. C. S., Tunved, P., Krejci, R., Ström, J., Hansson, H. C., Yoon, Y. J., Park, K. T., Becagli, S., Udisti, R., Onasch, T., Ódowd, C. D., Simó, R. and Harrison, R. M.: Arctic sea ice melt leads to atmospheric new particle formation, Sci. Rep., 7(1), 1–10, doi:10.1038/s41598-017-03328-1, 2017.

Dall´Osto, M., Simo, R., Harrison, R. M., Beddows, D. C. S., Saiz-Lopez, A., Lange, R., Skov, H., Nøjgaard, J. K., Nielsen, I. E. and Massling, A.: Abiotic and biotic sources influencing spring new particle formation in North East Greenland, Atmos. Environ., 190(July), 126–134, doi:10.1016/J.ATMOSENV.2018.07.019, 2018a.

Dall´Osto, M., Geels, C., Beddows, D. C. S., Boertmann, D., Lange, R., Nøjgaard, J. K., Harrison, R. M., Simo, R., Skov, H. and Massling, A.: Regions of open water and melting sea ice drive new particle formation in North East Greenland, Sci. Rep., 8(1), 6109, doi:10.1038/s41598-018-24426-8, 2018b.

Donahue, N. M., Epstein, S. A., Pandis, S. N. and Robinson, A. L.: A two-dimensional volatility basis set: 1. organic-aerosol mixing thermodynamics, Atmos. Chem. Phys.,

11(7), 3303–3318, doi:10.5194/acp-11-3303-2011, 2011.

Dunne, E. M., Gordon, H., Kurten, A., Almeida, J., Duplissy, J., Williamson, C., Ortega, I. K., Pringle, K. J., Adamov, A., Baltensperger, U., Barmet, P., Benduhn, F., Bianchi, F., Breitenlechner, M., Clarke, A., Curtius, J., Dommen, J., Donahue, N. M., Ehrhart, S., Flagan, R. C., Franchin, A., Guida, R., Hakala, J., Hansel, A., Heinritzi, M., Jokinen, T., Kangasluoma, J., Kirkby, J., Kulmala, M., Kupc, A., Lawler, M. J., Lehtipalo, K., Reddington, C. L. S., Riccobono, F., Richards, N. A. D., Rissanen, M. P., Rondo, L., Sarnela, N., Schobesberger, S., Sengupta, K., Simon, M., Sipilä, M., Smith, J. N., Stozkhov, Y., Tomé, A., Tröstl, J., Wagner, P. E., Williamson, C., Wimmer, D., Winkler, P. M., Yan, C. and Carslaw, K. S. .: Global atmospheric particle formation from CERN CLOUD measurements., Science (80-.)., 354(6316), 1119–1124, 2016.

Ellis, R. A., Murphy, J. G., Pattey, E., Van Haarlem, R., O'Brien, J. M. and Herndon, S. C.: Characterizing a Quantum Cascade Tunable Infrared Laser Differential Absorption Spectrometer (QC-TILDAS) for measurements of atmospheric ammonia, Atmos. Meas. Tech., 3(2), 397–406, doi:10.5194/amt-3-397-2010, 2010.

Facchini, M. C., Decesari, S., Rinaldi, M., Carbone, C., Finessi, E., Mircea, M., Fuzzi, S., Moretti, F., Tagliavini, E., Ceburnis, D. and O'Dowd, C. D.: Important Source of Marine Secondary Organic Aerosol from Biogenic Amines, Environ. Sci. Technol., 42(24), 9116–9121, doi:10.1021/es8018385, 2008.

Fairlie, T. D., Jacob, D. J. and Park, R. J.: The impact of transpacific transport of mineral dust in the United States, Atmos. Environ., 41(6), 1251–1266, doi:10.1016/j.atmosenv.2006.09.048, 2007.

Fisher, J. A., Jacob, D. J., Wang, Q., Bahreini, R., Carouge, C. C., Cubison, M. J., Dibb, J. E., Diehl, T., Jimenez, J. L., Leibensperger, E. M., Lu, Z., Meinders, M. B. J., Pye, H. O. T., Quinn, P. K., Sharma, S., Streets, D. G., van Donkelaar, A. and Yantosca, R. M.: Sources, distribution, and acidity of sulfate-ammonium aerosol in the Arctic in winter-spring, Atmos. Environ., 45(39), 7301–7318, doi:10.1016/j.atmosenv.2011.08.030, 2011.

Fogal, P. F., LeBlanc, L. M. and Drummond, J. R.: The Polar Environment Atmospheric Research Laboratory (PEARL): Sounding the Atmosphere at 80 North, Arctic, 66(3), 377–386 [online] Available from: http://www.jstor.org/stable/23594645, 2013.

Freud, E., Krejci, R., Tunved, P., Leaitch, R., Nguyen, Q. T., Massling, A., Skov, H. and Barrie, L.: Pan-Arctic aerosol number size distributions: Seasonality and transport patterns, Atmos. Chem. Phys., 17(13), 8101–8128, doi:10.5194/acp-17-8101-2017, 2017.

Fuchs, N. A.: The mechanics of aerosols. By N. A. Fuchs. Translated by R. E. Daisley and Marina Fuchs; Edited by C. N. Davies. London (Pergamon Press), 1964. Pp. xiv, 408; 82 Figures; 40 Tables. £6, Q. J. R. Meteorol. Soc., 91(388), 249, doi:10.1002/qj.49709138822, 1964.

Gantt, B. and Meskhidze, N.: The physical and chemical characteristics of marine primary organic aerosol: A review, Atmos. Chem. Phys., 13(8), 3979–3996, doi:10.5194/acp-13-3979-2013, 2013.

Garrett, T. J., Brattström, S., Sharma, S., Worthy, D. E. J. and Novelli, P.: The role of scavenging in the seasonal transport of black carbon and sulfate to the Arctic, Geophys. Res. Lett., 38(16), 1–6, doi:10.1029/2011GL048221, 2011.

Ghahremaninezhad, R., Norman, A. L., Abbatt, J. P. D., Levasseur, M. and Thomas, J. L.: Biogenic, anthropogenic and sea salt sulfate size-segregated aerosols in the Arctic summer, Atmos. Chem. Phys., 16(8), 5191–5202, doi:10.5194/acp-16-5191-2016, 2016.

Ghahremaninezhad, R., Norman, A. L., Croft, B., Martin, R. V., Pierce, J. R., Burkart, J., Rempillo, O., Bozem, H., Kunkel, D., Thomas, J. L., Aliabadi, A. A., Wentworth, G. R., Levasseur, M., Staebler, R. M., Sharma, S. and Richard Leaitch, W.: Boundary layer and free-Tropospheric dimethyl sulfide in the Arctic spring and summer, Atmos. Chem. Phys., 17(14), 8757–8770, doi:10.5194/acp-17-8757-2017, 2017.

Giamarelou, M., Eleftheriadis, K., Nyeki, S., Tunved, P., Torseth, K. and Biskos, G.: Indirect evidence of the composition of nucleation mode particles in the high Arctic, J. Geophys. Res. Atmos., 121, 965–975, doi:10.1002/2015JD023646, 2016.

Giglio, L., Randerson, J. T. and Van Der Werf, G. R.: Analysis of daily, monthly, and annual burned area using the fourth-generation global fire emissions database (GFED4), J. Geophys. Res. Biogeosciences, 118(1), 317–328, doi:10.1002/jgrg.20042, 2013.

Gordon, H., Kirkby, J., Baltensperger, U., Bianchi, F., Breitenlechner, M., Curtius, J., Dias, A., Dommen, J., Donahue, N. M., Dunne, E. M., Duplissy, J., Ehrhart, S., Flagan, R. C., Frege, C., Fuchs, C., Hansel, A., Hoyle, C. R., Kulmala, M., Kürten, A., Lehtipalo, K., Makhmutov, V., Molteni, U., Rissanen, M. P., Stozkhov, Y., Tröstl, J., Tsagkogeorgas, G., Wagner, R., Williamson, C., Wimmer, D., Winkler, P. M., Yan, C. and Carslaw, K. S.: Causes and importance of new particle formation in the present-day and preindustrial atmospheres, J. Geophys. Res. Atmos., 122(16), 8739–8760, doi:10.1002/2017JD026844, 2017.

Gourdal, M., Lizotte, M., Massé, G., Gosselin, M., Scarratt, M. and Levasseur, M.: Dimethylsulfide dynamics in first-year sea ice melt ponds in the Canadian Arctic Archipelago, Biogeosciences, 15, 3169–3188, doi:10.5194/bg-2017-432, 2018.

Grythe, H., Ström, J., Krejci, R., Quinn, P. and Stohl, A.: A review of sea-spray aerosol source functions using a large global set of sea salt aerosol concentration measurements, Atmos. Chem. Phys., 14(3), 1277–1297, doi:10.5194/acp-14-1277-2014, 2014.

Gunsch, M. J., Kirpes, R. M., Kolesar, K. R., Barrett, T. E., China, S., Sheesley, R. J., Laskin, A., Wiedensohler, A., Tuch, T. and Pratt, K. A.: Contributions of transported Prudhoe Bay oil field emissions to the aerosol population in Utqiaġvik, Alaska, Atmos.

Chem. Phys., 17(17), 10879–10892, doi:10.5194/acp-17-10879-2017, 2017.

Hayashida, H., Steiner, N., Monahan, A., Galindo, V., Lizotte, M. and Levasseur, M.: Implications of sea-ice biogeochemistry for oceanic production and emissions of dimethyl sulfide in the Arctic, , 3129–3155, 2017.

Hegg, D. A., Hobbs, P. V, Gass, S., Nance, J. D. and Rangno, A. L.: Aerosol measurements in the Arctic relevant to direct and indirect radiative forcing, J. Geophys. Res., 101(D18), 23,349-23,363, 1996.

Heintzenberg, J. and Leck, C.: The summer aerosol in the central Arctic 1991-2008: Did it change or not?, Atmos. Chem. Phys., 12(9), 3969–3983, doi:10.5194/acp-12-3969-2012, 2012.

Heintzenberg, J., Leck, C. and Tunved, P.: Potential source regions and processes of aerosol in the summer Arctic, Atmos. Chem. Phys., 15(11), 6487–6502, doi:10.5194/acp-15-6487-2015, 2015.

Heintzenberg, J., Tunved, P., Galí, M. and Leck, C.: New particle formation in the Svalbard region 2006-2015, Atmos. Chem. Phys., 17(10), 6153–6175, doi:10.5194/acp-17-6153-2017, 2017.

Hodshire, A. L., Palm, B. B., Alexander, M. L., Bian, Q., Campuzano-Jost, P., Cross, E. S., Day, D. A., de Sá, S. S., Guenther, A. B., Hansel, A., Hunter, J. F., Jud, W., Karl, T., Kim, S., Kroll, J. H., Park, J.-H., Peng, Z., Seco, R., Smith, J. N., Jimenez, J. L. and Pierce, J. R.: Constraining nucleation, condensation, and chemistry in oxidation flow reactors using size-distribution measurements and aerosol microphysical modelling, Atmos. Chem. Phys. Discuss., (May), 1–53, doi:10.5194/acp-2018-223, 2018.

Hodshire, A. L., Kodros, J. K., Croft, B., Campuzano-Jost, P., Nault, B. A., Schroder, J. C., Jimenez, J.-L. and Pierce, J. R.: The potential role of methansulfonic acid (MSA) in aerosol formation and growth and the associated radiative forcings, (in prep.), 2018.

Huang, L., Brook, J. R., Zhang, W., Li, S. M., Graham, L., Ernst, D., Chivulescu, A. and Lu, G.: Stable isotope measurements of carbon fractions (OC/EC) in airborne particulate: A new dimension for source characterization and apportionment, Atmos. Environ., 40, 2690-2705, 2006.

Iacono, M. J., Delamere, J. S., Mlawer, E. J., Shephard, M. W., Clough, S. A. and Collins, W. D.: Radiative forcing by long-lived greenhouse gases: Calculations with the AER radiative transfer models, J. Geophys. Res. Atmos., 113(13), 2–9, doi:10.1029/2008JD009944, 2008.

Jaeglé, L., Quinn, P. K., Bates, T. S., Alexander, B. and Lin, J. T.: Global distribution of sea salt aerosols: New constraints from in situ and remote sensing observations, Atmos. Chem. Phys., 11(7), 3137–3157, doi:10.5194/acp-11-3137-2011, 2011.

Johnson, M. T.: A numerical scheme to calculate temperature and salinity dependent air-water transfer velocities for any gas, Ocean Sci., 6(4), 913–932, doi:10.5194/os-6-913-2010, 2010.

Karl, M., Leck, C., Coz, E. and Heintzenberg, J.: Marine nanogels as a source of atmospheric nanoparticles in the high Arctic, Geophys. Res. Lett., 40(14), 3738–3743, doi:10.1002/grl.50661, 2013.

Kerminen, V. M., Anttila, T., Lehtinen, K. E. J. and Kulmala, M.: Parameterization for atmospheric new-particle formation: Application to a system involving sulfuric acid and condensable water-soluble organic vapors, Aerosol Sci. Technol., 38(10), 1001–1008, doi:10.1080/027868290519085, 2004.

Kim, P. S., Jacob, D. J., Fisher, J. A., Travis, K., Yu, K., Zhu, L., Yantosca, R. M., Sulprizio, M. P., Jimenez, J. L., Campuzano-Jost, P., Froyd, K. D., Liao, J., Hair, J. W., Fenn, M. A., Butler, C. F., Wagner, N. L., Gordon, T. D., Welti, A., Wennberg, P. O., Crounse, J. D., St. Clair, J. M., Teng, A. P., Millet, D. B., Schwarz, J. P., Markovic, M. Z. and Perring, A. E.: Sources, seasonality, and trends of Southeast US aerosol: An integrated analysis of surface, aircraft, and satellite observations with the GEOS-Chem chemical transport model, Atmos. Chem. Phys., 15, 10411-10433, doi:10.5194/acpd-15-10411-2015, 2015.

Kirkby, J., Curtius, J., Almeida, J., Dunne, E., Duplissy, J., Ehrhart, S., Franchin, A., Gagné, S., Ickes, L., Kürten, A., Kupc, A., Metzger, A., Riccobono, F., Rondo, L., Schobesberger, S., Tsagkogeorgas, G., Wimmer, D., Amorim, A., Bianchi, F., Breitenlechner, M., David, A., Dommen, J., Downard, A., Ehn, M., Flagan, R. C., Haider, S., Hansel, A., Hauser, D., Jud, W., Junninen, H., Kreissl, F., Kvashin, A., Laaksonen, A., Lehtipalo, K., Lima, J., Lovejoy, E. R., Makhmutov, V., Mathot, S., Mikkilä, J., Minginette, P., Mogo, S., Nieminen, T., Onnela, A., Pereira, P., Petäjä, T., Schnitzhofer, R., Seinfeld, J. H., Sipilä, M., Stozhkov, Y., Stratmann, F., Tomé, A., Vanhanen, J., Viisanen, Y., Vrtala, A., Wagner, P. E., Walther, H., Weingartner, E., Wex, H., Winkler, P. M., Carslaw, K. S., Worsnop, D. R., Baltensperger, U. and Kulmala, M.: Role of sulphuric acid, ammonia and galactic cosmic rays in atmospheric aerosol nucleation, Nature, 476(7361), 429–435, doi:10.1038/nature10343, 2011.

Kodros, J. K. and Pierce, J. R.: Important global and regional differences in aerosol cloud-albedo effect estimates between simulations with and without prognostic aerosol microphysics, J. Geophys. Res., 122(7), 4003–4018, doi:10.1002/2016JD025886, 2017.

Kodros, J. K., Cucinotta, R., Ridley, D. A., Wiedinmyer, C. and Pierce, J. R.: The aerosol radiative effects of uncontrolled combustion of domestic waste, Atmos. Chem. Phys., 16(11), 6771–6784, doi:10.5194/acp-16-6771-2016, 2016.

Kolesar, K. R., Cellini, J., Peterson, P. K., Jefferson, A., Tuch, T., Birmili, W., Wiedensohler, A. and Pratt, K. A.: Effect of Prudhoe Bay emissions on atmospheric

aerosol growth events observed in Utqiaġvik (Barrow), Alaska, Atmos. Environ., 152, 146–155, doi:https://doi.org/10.1016/j.atmosenv.2016.12.019, 2017.

Köllner, F., Schneider, J., Willis, M., Klimach, T., Helleis, F., Bozem, H., Kunkel, D., Hoor, P., Burkart, J., Richard Leaitch, W., Aliabadi, A. A., Abbatt, J. P. D., Herber, A. B. and Borrmann, S.: Particulate trimethylamine in the summertime Canadian high Arctic lower troposphere, Atmos. Chem. Phys., 17(22), 13747–13766, doi:10.5194/acp-17-13747-2017, 2017.

Korhonen, H., Carslaw, K. S., Spracklen, D. V., Ridley, D. A. and Ström, J.: A global model study of processes controlling aerosol size distributions in the Arctic spring and summer, J. Geophys. Res., 113(D8), D08211, doi:10.1029/2007JD009114, 2008.

Lana, A., Bell, T. G., Simó, R., Vallina, S. M., Ballabrera-Poy, J., Kettle, A. J., Dachs, J., Bopp, L., Saltzman, E. S., Stefels, J., Johnson, J. E. and Liss, P. S.: An updated climatology of surface dimethlysulfide concentrations and emission fluxes in the global ocean, Global Biogeochem. Cycles, 25(1), 1–17, doi:10.1029/2010GB003850, 2011.

Law, K. S. and Stohl, A.: Arctic Air Pollution: Orgins and Impacts, Science, 315(March), 1537–1540, 2007.

Leaitch, R. W., Russell, L. M., Liu, J., Kolonjari, F., Toom, D., Huang, L., Sharma, S., Chivulescu, A., Veber, D. and Zhang, W.: Organic functional groups in the submicron aerosol at 82.5 degrees N, 62.5 degrees W from 2012 to 2014, Atmos. Chem. Phys., 18, 3269–3287, doi:10.5194/acp-18-3269-2018, 2018.

Leaitch, W. R., Sharma, S., Huang, L., Toom-Sauntry, D., Chivulescu, A., Macdonald, A. M., von Salzen, K., Pierce, J. R., Bertram, A. K., Schroder, J. C., Shantz, N. C., Chang, R. Y.-W. and Norman, A.-L.: Dimethyl sulfide control of the clean summertime Arctic aerosol and cloud, Elem. Sci. Anthr., 1, 000017, doi:10.12952/journal.elementa.000017, 2013.

Leaitch, W. R., Korolev, A., Aliabadi, A. A., Burkart, J., Willis, M. D., Abbatt, J. P. D., Bozem, H., Hoor, P., Köllner, F., Schneider, J., Herber, A., Konrad, C. and Brauner, R.: Effects of 20-100nm particles on liquid clouds in the clean summertime Arctic, Atmos. Chem. Phys., 16(17), 11107–11124, doi:10.5194/acp-16-11107-2016, 2016.

Leck, C. and Bigg, E. K.: New particle formation of marine biological origin, Aerosol Sci. Technol., 44(7), 570–577, doi:10.1080/02786826.2010.481222, 2010.

Lee, Y. H. and Adams, P. J.: A fast and efficient version of the TwO-Moment Aerosol Sectional (TOMAS) global aerosol microphysics model, Aerosol Sci. Technol., 46(6), 678–689, doi:10.1080/02786826.2011.643259, 2012.

Li, M., Zhang, Q., Kurokawa, J. I., Woo, J. H., He, K., Lu, Z., Ohara, T., Song, Y., Streets, D. G., Carmichael, G. R., Cheng, Y., Hong, C., Huo, H., Jiang, X., Kang, S., Liu,

F., Su, H. and Zheng, B.: MIX: A mosaic Asian anthropogenic emission inventory under the international collaboration framework of the MICS-Asia and HTAP, Atmos. Chem. Phys., 17(2), 935–963, doi:10.5194/acp-17-935-2017, 2017.

Li, S.-M. and Barrie, L. a.: Biogenic sulfur aerosol in the Arctic troposphere: 1. Contributions to total sulfate, J. Geophys. Res., 98(D11), 20613, doi:10.1029/93JD02234, 1993.

Liu, H., Jacob, D. J., Bey, I. and Yantosca, R. M.: Constraints from210Pb and7Be on wet deposition and transport in a global three-dimensional chemical tracer model driven by assimilated meteorological fields, J. Geophys. Res. Atmos., 106(D11), 12109–12128, doi:10.1029/2000JD900839, 2001.

Liu, P., Li, Y. J., Wang, Y., Gilles, M. K., Zaveri, R. A., Bertram, A. K. and Martin, S. T.: Lability of secondary organic particulate matter, Proc. Natl. Acad. Sci., 113(45), 12643–12648, doi:10.1073/pnas.1603138113, 2016.

Lohmann, U. and Feichter, J.: Global indirect aerosol effects: a review, Atmos. Chem. Phys., 5, 715–737, doi:10.5194/acpd-4-7561-2004, 2005.

Lutsch, E., Dammers, E., Conway, S. and Strong, K.: Long-range Transport of NH_3, CO, HCN and C_2H_6 from the 2014 Canadian Wildfires, Geophys. Res. Lett., 1–12, doi:10.1002/2016GL070114, 2016.

Mårtensson, E. M., Nilsson, E. D., de Leeuw, G., Cohen, L. H. and Hansson, H.-C.: Laboratory simulations and parameterization of the primary marine aerosol production, J. Geophys. Res. Atmos., 108(D9), n/a-n/a, doi:10.1029/2002JD002263, 2003.

McFarquhar, G. M., Ghan, S., Verlinde, J., Korolev, A., Strapp, J. W., Schmid, B., Tomlinson, J. M., Wolde, M., Brooks, S. D., Cziczo, D., Dubey, M. K., Fan, J., Flynn, C., Gultepe, I., Hubbe, J., Gilles, M. K., Laskin, A., Lawson, P., Leaitch, W. R., Liu, P., Liu, X., Lubin, D., Mazzoleni, C., MacDonald, A. M., Moffet, R. C., Morrison, H., Ovchinnikov, M., Shupe, M. D., Turner, D. D., Xie, S., Zelenyuk, A., Bae, K., Freer, M. and Glen, A.: Indirect and semi-direct aerosol campaign: The impact of arctic aerosols on clouds, Bull. Am. Meteorol. Soc., 92(2), 183–201, doi:10.1175/2010BAMS2935.1, 2011.

Mungall, E. L., Croft, B., Lizotte, M., Thomas, J. L., Murphy, J. G., Levasseur, M., Martin, R. V., Wentzell, J. J. B., Liggio, J. and Abbatt, J. P. D.: Dimethyl sulfide in the summertime Arctic atmosphere: Measurements and source sensitivity simulations, Atmos. Chem. Phys., 16(11), 6665–6680, doi:10.5194/acp-16-6665-2016, 2016.

Mungall, E. L., Abbatt, J. P. D., Wentzell, J. J. B., Lee, A. K. Y., Thomas, J. L., Blais, M., Gosselin, M., Miller, L. A., Papakyriakou, T., Willis, M. D. and Liggio, J.: Microlayer source of oxygenated volatile organic compounds in the summertime marine Arctic boundary layer, Proc. Natl. Acad. Sci., 114(24), 6203–6208, doi:10.1073/pnas.1620571114, 2017.

Murphy, J.G., Moravek, A., Wentworth, G.R., et al.: Observational constraints on the atmospheric ammonia budget in the Canadian Arctic Archipelago, (in prep.), 2018.

Napari, I., Noppel, M., Vehkamaki, H. and Kulmala, M.: Parametrization of ternary nucleation rates for H2SO4-NH3-H2O vapors, J. Geophys. Res. Atmos., 107(19), 2–7, doi:10.1029/2002JD002132, 2002.

Nguyen, Q. T., Glasius, M., Sørensen, L. L., Jensen, B., Skov, H., Birmili, W., Wiedensohler, A., Kristensson, A., Nøjgaard, J. K. and Massling, A.: Seasonal variation of atmospheric particle number concentrations, new particle formation and atmospheric oxidation capacity at the high Arctic site Villum Research Station, Station Nord, Atmos. Chem. Phys., 16(17), 11319–11336, doi:10.5194/acp-16-11319-2016, 2016.

Olenius, T., Kupiainen-Määttä, O., Ortega, I. K., Kurtén, T. and Vehkamäki, H.: Free energy barrier in the growth of sulfuric acid-ammonia and sulfuric acid-dimethylamine clusters, J. Chem. Phys., 139(8), doi:10.1063/1.4819024, 2013.

Petters, M. D. and Kreidenweis, S. M.: A single parameter representation of hygroscopic growth and cloud condensation nucleus activity-Part 3: Including surfactant partitioning, Atmos. Chem. Phys., 7, 1961–1971, doi:10.5194/acp-13-1081-2013, 2007.

Philip, S., Martin, R. V., Pierce, J. R., Jimenez, J. L., Zhang, Q., Canagaratna, M. R., Spracklen, D. V., Nowlan, C. R., Lamsal, L. N., Cooper, M. J. and Krotkov, N. A.: Spatially and seasonally resolved estimate of the ratio of organic mass to organic carbon, Atmos. Environ., 87, 34–40, doi:10.1016/j.atmosenv.2013.11.065, 2014.

Pierce, J. R., Riipinen, I., Kulmala, M., Ehn, M., Petäjä, T., Junninen, H., Worsnop, D. R. and Donahue, N. M.: Quantification of the volatility of secondary organic compounds in ultrafine particles during nucleation events, Atmos. Chem. Phys., 11(17), 9019–9036, doi:10.5194/acp-11-9019-2011, 2011.

Pierce, J. R., Croft, B., Kodros, J. K., D'Andrea, S. D. and Martin, R. V.: The importance of interstitial particle scavenging by cloud droplets in shaping the remote aerosol size distribution and global aerosol-climate effects, Atmos. Chem. Phys., 15(11), 6147–6158, doi:10.5194/acp-15-6147-2015, 2015.

Polissar, A. V, Hopke, P. K. and Harris, J. M.: Source Regions for Atmospheric Aerosol Measured at Barrow, Alaska, Environ. Sci. Technol., 35(21), 4214–4226, doi:10.1021/es0107529, 2001.

Prather, K. A., Bertram, T. H., Grassian, V. H., Deane, G. B., Stokes, M. D., DeMott, P. J., Aluwihare, L. I., Palenik, B. P., Azam, F., Seinfeld, J. H., Moffet, R. C., Molina, M. J., Cappa, C. D., Geiger, F. M., Roberts, G. C., Russell, L. M., Ault, A. P., Baltrusaitis, J., Collins, D. B., Corrigan, C. E., Cuadra-Rodriguez, L. A., Ebben, C. J., Forestieri, S. D., Guasco, T. L., Hersey, S. P., Kim, M. J., Lambert, W. F., Modini, R. L., Mui, W., Pedler,

B. E., Ruppel, M. J., Ryder, O. S., Schoepp, N. G., Sullivan, R. C. and Zhao, D.: Bringing the ocean into the laboratory to probe the chemical complexity of sea spray aerosol, Proc. Natl. Acad. Sci., 110(19), 7550–7555, doi:10.1073/pnas.1300262110, 2013.

Quinn, P. K., Miller, T. L., Bates, T. S., Ogren, J. A., Andrews, E. and Shaw, G. E.: A 3-year record of simultaneously measured aerosol chemical and optical properties at Barrow, Alaska, J. Geophys. Res. Atmos., 107(D11), doi:10.1029/2001JD001248, 2002.

Quinn, P. K., Collins, D. B., Grassian, V. H., Prather, K. A. and Bates, T. S.: Chemistry and Related Properties of Freshly Emitted Sea Spray Aerosol, Chem. Rev., 115(10), 4383–4399, doi:10.1021/cr500713g, 2015.

Rap, A., Scott, C. E., Spracklen, D. V., Bellouin, N., Forster, P. M., Carslaw, K. S., Schmidt, A. and Mann, G.: Natural aerosol direct and indirect radiative effects, Geophys. Res. Lett., 40(12), 3297–3301, doi:10.1002/grl.50441, 2013.

Riccobono, F., Schobesberger, S., Scott, C. E., Dommen, J., Ortega, I. K., Rondo, L., Almeida, J., Amorim, A., Bianchi, F., Breitenlechner, M., David, A., Downard, A., Dunne, E. M., Duplissy, J., Ehrhart, S., Flagan, R. C., Franchin, A., Hansel, A., Junninen, H., Kajos, M., Keskinen, H., Kupc, A., Kupiainen, O., Kürten, A., Kurtén, T., Kvashin, A. N., Laaksonen, A., Lehtipalo, K., Makhmutov, V., Mathot, S., Nieminen, T., Olenius, T., Onnela, A., Petäjä, T., Praplan, A. P., Santos, F. D., Schallhart, S., Seinfeld, J. H., Sipilä, M., Spracklen, D. V, Stozhkov, Y., Stratmann, F., Tomé, A., Tsagkogeorgas, G., Vaattovaara, P., Vehkamäki, H., Viisanen, Y., Vrtala, A., Wagner, P. E., Weingartner, E., Wex, H., Wimmer, D., Carslaw, K. S., Curtius, J., Donahue, N. M., Kirkby, J., Kulmala, M., Worsnop, D. R., Baltensperger, U. U. ., Schobesberger, S., Scott, C. E., Dommen, J., Ortega, I. K., Rondo, L., Almeida, J., Amorim, A., Bianchi, F., Breitenlechner, M., David, A., Downard, A., Dunne, E. M., Duplissy, J., Ehrhart, S., Flagan, R. C., Franchin, A., Hansel, A., Junninen, H., Kajos, M., Keskinen, H., Kupc, A., Kürten, A., Kvashin, A. N., Laaksonen, A., Lehtipalo, K., Makhmutov, V., Mathot, S., Nieminen, T., Onnela, A., Petäjä, T., Praplan, A. P., Santos, F. D., Schallhart, S., Seinfeld, J. H., Sipilä, M., Spracklen, D. V, Stozhkov, Y., Stratmann, F., Tomé, A., Tsagkogeorgas, G., et al.: Oxidation Products of Biogenic Emissions Contribute to Nucleation of Atmospheric Particles, Science, 344(May), 717–721 [online] Available from: http://www.sciencemag.org/content/344/6185/717.abstract, 2014.

Riddick, S. N., Dragosits, U., Blackall, T. D., Daunt, F., Wanless, S. and Sutton, M. A.: The global distribution of ammonia emissions from seabird colonies, Atmos. Environ., 55, 319–327, doi:10.1016/j.atmosenv.2012.02.052, 2012a.

Riddick, S. N. Dragosits, U., Blackall, T.D., Daunt, F., Wanless, S., Sutton, M.A.: Global ammonia emissions from seabirds. NERC Environmental Information Data Centre, https://doi.org/10.5285/c9e802b3-43c8-4b36-a3a3-8861d9da8ea9, 2012b.

Riipinen, I., Pierce, J. R., Yli-Juuti, T., Nieminen, T., Häkkinen, S., Ehn, M., Junninen,

H., Lehtipalo, K., Petäjä, T., Slowik, J., Chang, R., Shantz, N. C., Abbatt, J., Leaitch, W. R., Kerminen, V. M., Worsnop, D. R., Pandis, S. N., Donahue, N. M. and Kulmala, M.: Organic condensation: A vital link connecting aerosol formation to cloud condensation nuclei (CCN) concentrations, Atmos. Chem. Phys., 11(8), 3865–3878, doi:10.5194/acp-11-3865-2011, 2011.

Rinaldi, M., Decesari, S., Finessi, E., Giulianelli, L., Carbone, C., Fuzzi, S., O'Dowd, C. D., Ceburnis, D. and Facchini, M. C.: Primary and Secondary Organic Marine Aerosol and Oceanic Biological Activity: Recent Results and New Perspectives for Future Studies, Adv. Meteorol., 2010, 1–10, doi:10.1155/2010/310682, 2010.

Russell, L. M.: Aerosol organic-mass-to-organic-carbon ratio measurements, Environ. Sci. Technol., 37(13), 2982–2987, doi:10.1021/es026123w, 2003.

Scott, C. E., Rap, A., Spracklen, D. V., Forster, P. M., Carslaw, K. S., Mann, G. W., Pringle, K. J., Kivekäs, N., Kulmala, M., Lihavainen, H. and Tunved, P.: The direct and indirect radiative effects of biogenic secondary organic aerosol, Atmos. Chem. Phys., 14(1), 447–470, doi:10.5194/acp-14-447-2014, 2014.

Sharma, S., Ishizawa, M., Chan, D., Lavoué, D., Andrews, E., Eleftheriadis, K. and Maksyutov, S.: 16-year simulation of arctic black carbon: Transport, source contribution, and sensitivity analysis on deposition, J. Geophys. Res. Atmos., 118(2), 943–964, doi:10.1029/2012JD017774, 2013.

Sharma, S., Richard Leaitch, W., Huang, L., Veber, D., Kolonjari, F., Zhang, W., Hanna, S. J., Bertram, A. K. and Ogren, J. A.: An evaluation of three methods for measuring black carbon in Alert, Canada, Atmos. Chem. Phys., 17(24), 15225–15243, doi:10.5194/acp-17-15225-2017, 2017.

Shindell, D. and Faluvegi, G.: Climate response to regional radiative forcing during the twentieth century, Nat. Geosci., 2(4), 294–300, doi:10.1038/ngeo473, 2009.

Skrzypek, G., Wojtuń, B., Richter, D., Jakubas, D., Wojczulanis-Jakubas, K. and Samecka-Cymerman, A.: Diversification of nitrogen sources in various tundra vegetation types in the high arctic, PLoS One, 10(9), 1–21, doi:10.1371/journal.pone.0136536, 2015.

Steinke, M., Hodapp, B., Subhan, R., Bell, T. G. and Martin-Creuzburg, D.: Flux of the biogenic volatiles isoprene and dimethyl sulfide from an oligotrophic lake, Sci. Rep., 8(1), 1–10, doi:10.1038/s41598-017-18923-5, 2018.

Stohl, A.: Characteristics of atmospheric transport into the Arctic troposphere, J. Geophys. Res. Atmos., 111(11), 1–17, doi:10.1029/2005JD006888, 2006.

Tokarek, T. W., Brownsey, D. K., Jordan, N., Garner, N. M., Ye, C. Z., Assad, F. V., Peace, A., Schiller, C. L., Mason, R. H., Vingarzan, R. and Osthoff, H. D.: Biogenic Emissions and Nocturnal Ozone Depletion Events at the Amphitrite Point Observatory on

Vancouver Island, Atmos. - Ocean, 55(2), 121–132, doi:10.1080/07055900.2017.1306687, 2017.

Tremblay, S., Picard, J.-C., Bachelder, J. O., Lutsch, E., Strong, K., Fogal, P., Leaitch, W. R., Sharma, S., Kolonjari, F., Cox, C. J., Chang, R. Y.-W. and Hayes, P. L.: Characterization of aerosol growth events over Ellesmere Island during summers of 2015 and 2016, Atmos. Chem. Phys. Discuss, 5194(May), 2018–428, doi:10.5194/acp-2018-428, 2018.

Tröstl, J., Chuang, W. K., Gordon, H., Heinritzi, M., Yan, C., Molteni, U., Ahlm, L., Frege, C., Bianchi, F., Wagner, R., Simon, M., Lehtipalo, K., Williamson, C., Craven, J. S., Duplissy, J., Adamov, A., Almeida, J., Bernhammer, A. K., Breitenlechner, M., Brilke, S., Dias, A., Ehrhart, S., Flagan, R. C., Franchin, A., Fuchs, C., Guida, R., Gysel, M., Hansel, A., Hoyle, C. R., Jokinen, T., Junninen, H., Kangasluoma, J., Keskinen, H., Kim, J., Krapf, M., Kürten, A., Laaksonen, A., Lawler, M., Leiminger, M., Mathot, S., Möhler, O., Nieminen, T., Onnela, A., Petäjä, T., Piel, F. M., Miettinen, P., Rissanen, M. P., Rondo, L., Sarnela, N., Schobesberger, S., Sengupta, K., Sipilä, M., Smith, J. N., Steiner, G., Tomè, A., Virtanen, A., Wagner, A. C., Weingartner, E., Wimmer, D., Winkler, P. M., Ye, P., Carslaw, K. S., Curtius, J., Dommen, J., Kirkby, J., Kulmala, M., Riipinen, I., Worsnop, D. R., Donahue, N. M. and Baltensperger, U.: The role of low-volatility organic compounds in initial particle growth in the atmosphere, Nature, 533(7604), 527–531, doi:10.1038/nature18271, 2016.

Tunved, P., Ström, J. and Krejci, R.: Arctic aerosol life cycle: Linking aerosol size distributions observed between 2000 and 2010 with air mass transport and precipitation at Zeppelin station, Ny-Ålesund, Svalbard, Atmos. Chem. Phys., 13(7), 3643–3660, doi:10.5194/acp-13-3643-2013, 2013.

Turpin, B. J. and Lim, H.-J.: Species Contributions to PM2 . 5 Mass Concentrations : Revisiting Common Assumptions for Estimating Organic Mass Species Contributions to PM2 . 5 Mass Concentrations : Revisiting Common Assumptions for Estimating Organic Mass, Aerosol Sci. Technol., 35, 602–610, doi:10.1080/02786820119445, 2001.

Walker, J. T., Robarge, W. P. and Austin, R.: Modeling of ammonia dry deposition to a pocosin landscape downwind of a large poultry facility, Agric. Ecosyst. Environ., 185, 161–175, doi:https://doi.org/10.1016/j.agee.2013.10.029, 2014.

Wang, Q., Jacob, D. J., Fisher, J. A., Mao, J., Leibensperger, E. M., Carouge, C. C., Le Sager, P., Kondo, Y., Jimenez, J. L., Cubison, M. J. and Doherty, S. J.: Sources of carbonaceous aerosols and deposited black carbon in the Arctic in winter-spring: Implications for radiative forcing, Atmos. Chem. Phys., 11(23), 12453–12473, doi:10.5194/acp-11-12453-2011, 2011.

Wentworth, G. R., Murphy, J. G., Gregoire, P. K., Cheyne, C. A. L., Tevlin, A. G. and Hems, R.: Soil-atmosphere exchange of ammonia in a non-fertilized grassland: Measured emission potentials and inferred fluxes, Biogeosciences, 11(20), 5675–5686,

doi:10.5194/bg-11-5675-2014, 2014.

Wentworth, G. R., Murphy, J. G., Croft, B., Martin, R. V., Pierce, J. R., Côté, J. S., Courchesne, I., Tremblay, J. É., Gagnon, J., Thomas, J. L., Sharma, S., Toom-Sauntry, D., Chivulescu, A., Levasseur, M. and Abbatt, J. P. D.: Ammonia in the summertime Arctic marine boundary layer: Sources, sinks, and implications, Atmos. Chem. Phys., 16(4), 1937–1953, doi:10.5194/acp-16-1937-2016, 2016.

Van Der Werf, G. R., Randerson, J. T., Giglio, L., Van Leeuwen, T. T., Chen, Y., Rogers, B. M., Mu, M., Van Marle, M. J. E., Morton, D. C., Collatz, G. J., Yokelson, R. J. and Kasibhatla, P. S.: Global fire emissions estimates during 1997-2016, Earth Syst. Sci. Data, 9(2), 697–720, doi:10.5194/essd-9-697-2017, 2017.

Wesely, M. L.: Parameterization of surface resistances to gaseous dry deposition in regional-scale numerical models, Atmos. Environ., 23, 1293–1304, 1989.

Willis, M. D., Burkart, J., Thomas, J. L., Köllner, F., Schneider, J., Bozem, H., Hoor, P. M., Aliabadi, A. A., Schulz, H., Herber, A. B., Leaitch, W. R. and Abbatt, J. P. D.: Growth of nucleation mode particles in the summertime Arctic: A case study, Atmos. Chem. Phys., 16(12), 7663–7679, doi:10.5194/acp-16-7663-2016, 2016.

Willis, M. D., Köllner, F., Burkart, J., Bozem, H., Thomas, J. L., Schneider, J., Aliabadi, A. A., Hoor, P. M., Schulz, H., Herber, A. B., Leaitch, W. R. and Abbatt, J. P. D.: Evidence for marine biogenic influence on summertime Arctic aerosol, Geophys. Res. Lett., 44(12), 6460–6470, doi:10.1002/2017GL073359, 2017.

Wilson, T. W., Ladino, L. A., Alpert, P. A., Breckels, M. N., Brooks, I. M., Browse, J., Burrows, S. M., Carslaw, K. S., Huffman, J. A., Judd, C., Kilthau, W. P., Mason, R. H., McFiggans, G., Miller, L. A., Najera, J. J., Polishchuk, E., Rae, S., Schiller, C. L., Si, M., Temprado, J. V., Whale, T. F., Wong, J. P. S., Wurl, O., Yakobi-Hancock, J. D., Abbatt, J. P. D., Aller, J. Y., Bertram, A. K., Knopf, D. A. and Murray, B. J.: A marine biogenic source of atmospheric ice-nucleating particles, Nature, 525(7568), 234–238, doi:10.1038/nature14986, 2015.

Xu, J. W., Martin, R. V., Morrow, A., Sharma, S., Huang, L., Richard Leaitch, W., Burkart, J., Schulz, H., Zanatta, M., Willis, M. D., Henze, D. K., Lee, C. J., Herber, A. B. and Abbatt, J. P. D.: Source attribution of Arctic black carbon constrained by aircraft and surface measurements, Atmos. Chem. Phys., 17(19), 11971–11989, doi:10.5194/acp-17-11971-2017, 2017.

Yang, Q., Bitz, C. M. and Doherty, S. J.: Offsetting effects of aerosols on Arctic and global climate in the late 20th century, Atmos. Chem. Phys., 14(8), 3969–3975, doi:10.5194/acp-14-3969-2014, 2014.

Ye, Q., Robinson, E. S., Ding, X., Ye, P., Sullivan, R. C. and Donahue, N. M.: Mixing of secondary organic aerosols versus relative humidity, Proc. Natl. Acad. Sci., 113(45),

12649–12654, doi:10.1073/pnas.1604536113, 2016.

Yu, H., Kaufman, Y. J., Chin, M., Feingold, G., Remer, L. A., Anderson, T. L., Balkanski, Y., Bellouin, N., Boucher, O., Christopher, S., DeCola, P., Kahn, R., Koch, D., Loeb, N., Reddy, M. S., Schulz, M., Takemura, T. and Zhou, M.: A review of measurement-based assessments of the aerosol direct radiative effect and forcing, Atmos. Chem. Phys., 6(3), 613–666, doi:10.5194/acp-6-613-2006, 2006.

Zábori, J., Rastak, N., Yoon, Y. J., Riipinen, I. and Ström, J.: Size-resolved cloud condensation nuclei concentration measurements in the Arctic: Two case studies from the summer of 2008, Atmos. Chem. Phys., 15(23), 13803–13817, doi:10.5194/acp-15-13803-2015, 2015.

Zender, C. S.: Mineral Dust Entrainment and Deposition (DEAD) model: Description and 1990s dust climatology, J. Geophys. Res., 108(D14), 4416, doi:10.1029/2002JD002775, 2003.